Using ground penetrating radar methods to investigate reinforced concrete structures

Using Ground-Penetrating Radar Methods to Investigate Reinforced Concrete Structures

Fabio TOSTI[1*] and Chiara FERRANTE[2]

[1]School of Computing and Engineering, University of West London (UWL), St Mary's Road, Ealing, London W5 5RF, UK. e-mail: Fabio.Tosti@uwl.ac.uk; Tel: +44 (0) 20 8231 2984; (*Corresponding Author); ORCID Id: 0000-0003-0291-9937

[2]Department of Engineering, Roma Tre University, Via Vito Volterra 62, 00146, Rome, Italy. e-mail: chiara.ferrante@uniroma3.it

Abstract

This paper provides an overview of the existing literature on the subject of Ground-Penetrating Radar (GPR) methods for the investigation of reinforced concrete structures. An overview of the use of concrete and reinforced concrete in civil engineering infrastructures is given. A review of the main destructive and non-destructive testing (NDT) methods in the field is presented, and an increase in the use of GPR to reinforced concrete structures is highlighted. It was also observed that research in some application areas has been predominantly or exclusively carried out at a laboratory scale, and that similarly, other more application-oriented research has been developed only on real-life structures. The effectiveness of GPR in these areas is demonstrated. Furthermore, a case study is presented on a new methodological and data processing approach for the assessment of reinforced concrete structures using a high-frequency dual-polarised antenna system. Results have proven the advantages of using the proposed methodology and GPR system in order to improve the detectability of rebars, including secondary bottom lines of reinforcement. The horizontal polarisation was proven to be more stable compared to the vertical. Finally, it has been demonstrated that a more accurate location of the rebars in a high-density grid mesh arrangement can be obtained by means of data migration processing with a scan spacing of 5 cm and wave velocity information through the use of the hyperbola fitting method from at least the 30% of targets.

Keywords: ground-penetrating radar (GPR); reinforced concrete structures; non-destructive assessment; standard test methods in concrete; data sampling methodology for migration; rebar location

1. INTRODUCTION

Reinforced concrete is a dominant structural material in construction engineering in many countries. The extensive use of reinforced concrete structures depends on a number of factors, such as i) a wide availability of reinforcing bars and concrete constituents (gravel or crushed rock, sand, water, and cement); ii) a relative ease in concrete construction; and iii) the economy of reinforced concrete compared with other construction materials.

Reinforced concrete is used in many types of building, in underground structures, water tanks, wind turbine foundations and towers, offshore oil exploration and production structures, dams, bridges, and also ships (Wight and MacGregor, 2012).

A kind of concrete was first used for the construction of structures in Crete during the Minoan civilisation, about 2000 B.C. This concrete-like material was not water resistant and, therefore, could not be used for exposed or underwater structures. Thousands of years later, the Pantheon's concrete dome was completed by the Romans in A.D. 126. The building still stands as the largest unsupported dome in the world with a diameter of 49 m, and is built with concrete made with broken bricks as aggregates.

In 1824, Portland cement was developed by Joseph Aspdin (Sharp, 2006) who mixed ground limestone and clay from different quarries and used a kiln to produce the cement. However, the material currently known as Portland cement was cretaed by I. C. Johnson in 1845. He found that the best cement resulted from the grinding of a hard clinker, produced when the mixture was overheated. In 1854, William Boutland Wilkinson of Newcastle patented a reinforced concrete floor (Moussard et al., 2017). The introduction of reinforcing bars allowed to cover the structural gaps of non-reinforced concrete, which is strong in terms of compression but weak in terms of tension. In fact, it is known that tensile stresses caused by loads, restrained shrinkage, or temperature changes create cracks when the tensile stress of a material is exceeded. In addition, an unreinforced beam can collapse very rapidly at the formation of first cracks. Conversely, reinforcing bars embedded in the concrete allow tension forces to form for moment equilibrium after the concrete is cracked. Prestressed concrete was introduced by Eugène Freyssinet more recently, in 1928, by putting reinforcement (i.e. pre-stressing tendons) into tension and concrete into compression (Billington, 2004). This allowed to delay the formation of cracks in the beam.

The construction of reinforced concrete members must follow a dedicated manufacturing process (Neville and Brooks, 1987). Reinforced concrete structures consist of a series of "members" that interact to support the loads placed on the structure. An overview of the various types of configuration and load transmission modes for these structures has been given by Wight and MacGregor (2012). The advantages of using reinforced concrete in place of other construction materials such as steel, masonry, or timber have been a subject of debate. The main benefits and disadvantages of using concrete structures are summarised in Tables 1 and 2 respectively.

61

62 **Table 1** Advantages of concrete structures

Consideration	Assessment
Availability	The foremost consideration is the wide availability of reinforcing bars and of the concrete constituents (gravel or crushed rock, sand, water, and cement) that can be easily found and transported to the construction site and, hence, it is preferred as a construction material in remote areas.
Economy	From an overall structural cost point of view, reinforced concrete constructions are cheaper compared to other construction materials in terms of cost of materials and the relative ease in concrete construction.
Suitability	From a shape point of view, concrete has the advantage that it is placed in plastic conditions and it allows to give the desired shape according to the structural function.
Fire resistance	Concrete buildings are fire resistant, with 1- to 3-hour fire rating without special fireproofing.
Rigidity	Concrete buildings have greater stiffness and mass that prevent the formation of oscillations and vibrations.
Low maintenance	Concrete buildings require less maintenance than buildings made of structural steel or timber members.

63

64 **Table 2** Drawbacks of concrete structures

Consideration	Assessment
Low tensile strength	Concrete is strong in compression and weak in tension. The tensile strength is about 1/10 of the compressive strength, therefore reinforcements are required when concrete is subject to tensile stresses.
Low strength per unit of weight or volume	Concrete has a compressive strength and a unit density of about 10% and 30% the steel, respectively. Therefore, a concrete structure requires a larger volume and a greater weight than a steel structure.
Forms	The construction process of concrete structures involves labour and time due to the use of more complex formworks and finishes compared to other types of structures.
Volume changes	At the curing stage, concrete is subject to a drying shrinkage that may cause cracking or unwanted deflections.
Energy used in manufacture	Cement used for concrete production is a high-energy material that results in high costs.
Environmental impact	● The high levels of CO_2 emissions at the production stage cover the 5% of the worldwide generation of CO_2. ● Loss of agricultural lands as well as visual impact caused by major concrete structures on some areas of outstanding natural beauty are elements of major concern. ● Care is necessary for the extraction of natural raw material components to avoid damage to the landscape.

65

66 A number of key processes may damage the integrity of a concrete structure, especially during the material's service life.
67 Corrosion associated with reinforcing bars is the most significant factor contributing to structural damage (Beena et al.,
68 2017). It is usually caused by excessive moisture content and chloride ions in the parts of the concrete adjacent to the

reinforcing steel. The early stage of corrosion is generally known as the initial passivity stage. Reinforcing bars are rapidly attacked by acidic, wet corrosion, yield expansive, hydrated corrosion products. These can in turn accelerate the formation of cracks in the surrounding concrete. The oxidation products occupy a larger volume than the original intact steel and so the internal expansive stresses lead to cracking and debonding. This occurrence is commonly known as the delamination of concrete cover material from the reinforcing layer (Neville and Brooks, 1987; Meng et al., 2020).

Within this framework, a comprehensive assessment and monitoring of concrete structures is required in order to properly identify the type and stage of decay. Traditional methods for investigating reinforced structures rely mostly on the use of destructive techniques (Tosti and Slob, 2015). In this regard, the most frequently used methods are coring, drilling or otherwise removing part of the structure to allow inner visual inspections of rebar conditions. Although destructive techniques provide accurate information, they are expensive, time-consuming and significant only at the point of acquisition. In addition, local damage at the sampling point may spread and can accelerate the process of decay.

In view of the above, non-destructive testing (NDT) methods are gaining momentum in the assessment of civil engineering structures and infrastructures as fundamental tools for providing a more comprehensive survey programme (Loizos and Plati, 2007; Plati et al., 2014; Fontul et al., 2018). NDT methods have taken hold in the field of concrete structures in view of the increasing accuracy and effectiveness of their measurements.

There exists a wide spectrum of NDT techniques based on different theoretical principles and the production of various sets of information regarding the physical properties of a structure. In general, it is worth considering five major factors for the planning of a non-destructive survey (McCann and Forde, 2001). These are i) the required depth of penetration into the structure; ii) the vertical and lateral resolution required for the anticipated targets; iii) the contrast in the physical properties between the target and its surroundings; iv) the signal-to-noise ratio for the physical property measured on the structure under investigation; v) the historic information concerning the methods used in the construction of the structure. The major NDT methods used for the investigation of reinforced concrete structures are the sonic/ultrasonic methods, the infrared thermography, radiography and the electromagnetic (EM) methods (e.g. radar-based methods).

Non-destructive sonic/ultrasonic testing methods have been used for the past thirty years for the assessment of civil engineering structures and materials (McCann and Forde, 2001). These methods are based on the transmission and reflection of mechanical stress waves at sonic and ultrasonic frequencies through a medium. In more detail, a sonic transmission method involves the passing of a compression wave at frequencies between 500 Hz and 10 kHz, generated by the impact of a force hammer with the structure. Effects of the wave are received by an accelerometer located on the opposite side of the force hammer. An improvement of the sonic method is sonic tomography, where tests are not restricted to being carried out along a path perpendicular to the surface of the medium. In the sonic reflection method, both the initiation and the reception stage of a wave are performed on the same face of the medium's surface. Finally,

ultrasonic methods rely on the use of ultrasonic waves at frequencies above 20 kHz. This method was the first non-destructive technique developed for the testing of concrete. Nevertheless, the ultrasonic method is less practical in concrete structures due to the higher attenuation characteristics of concrete and hence lower frequency signals are needed to obtain a reasonable penetration. Another major issue with using ultrasonic methods is the scattering of both incident and reflected waves, due to the different types of materials used in the mix.

Infrared thermography is a technique that allows heat at any temperature to be converted into a thermal image using a specific scanning camera (Stanley and Balendran, 1995). With this technology, it is possible to assess buildings or structures with defects (e.g. debonding render and mosaic or delaminating concrete) with regards to different infrared radiations. A concrete surface that is free of defects appears as relatively uniform in a thermal camera. On the other hand, cracks or other surface defects are displayed in red as they heat up faster under solar irradiation.

Radiography is another NDT method that uses x-rays, gamma rays and neutron rays, which are types of very short wavelength EM radiations. It is based on the detection and recording of the wave radiation penetrating through a medium. The amount of absorption depends on the density and thickness of the material as well as on the characteristics of the radiation. The radiation passing through the medium is recorded on a film or a sensitised paper and viewed on a screen. The sensitivity of the radiography depends on several factors, as the thickness and the direction of the radiation with respect to the defect: the best results can be obtained when a defect is significantly thick in a parallel direction to the radiation beam. The main application of radiographic techniques is the welds and castings inspection (Mishin, 1997**)**.

EM methods are based on electromagnetic theory, described by the Maxwell's equations, and the material properties, quantified by constitutive relationships. These methods use the radar technology that is being spread quickly among NDT methods in the field of structural engineering, including applications on reinforced concrete structures.

In more detail, ground-penetrating radar (GPR) is a geophysical inspection method used to scan the subsurface in many application areas (Lai et al., 2009), including concrete structures such as buildings, dams (Rhim, 2001) and bridges (Kohl, 2006). GPR is a relatively new geophysical technique that has seen major advances in the last decade (Gizzi and Leucci, 2018), especially for civil engineering applications (Annan, 2004; Daniels, 2004). The working principle of the GPR technique is based on sending a short-duration EM wave and recording arrival time, amplitude and phase of the back-reflected signal. These outputs are dependent on the GPR characteristics and the properties of the host material.

According to Burgey et al. (2003), GPR has several key practical advantages as opposed to other geophysical NDT methods. It is in fact a piece of light and portable equipment where no coupling medium or special safety precautions are required, in terms of emission of microwaves. In addition, GPR allows some of the most critical features in reinforced concrete structures to be detected.

The present work reports an overview of the use of GPR methods for the investigation of reinforced concrete structures. Section 2 discusses the main international standard test methods and guidelines. The theoretical background and working principles of the GPR technology with an overview of the main applications in reinforced concrete structures are given in Section 3. Section 4 reports an historical review of research methods on the use of GPR in this subject area. Section 5 presents a case study on a new methodological and data processing approach for the assessment of reinforced concrete structures. Conclusions are presented in the last section of the paper.

2. STANDARD TEST METHODS AND GUIDELINES

This Section reports a selection of principal destructive, partially-destructive and non-destructive standard test methods for concrete and reinforced concrete assessment. Discussed standards have been released by the American Society for Testing and Materials (ASTM), the American Concrete Institute (ACI) and the British Standards Institution (BSI).

Destructive testing methods require samples of the investigated structural element to be collected, usually in the form of cores. These are assessed in the laboratory for strength analyses and other physical tests as well as visual, petrographic and chemical investigations. Partially-destructive testing methods include tests requiring a minor level of damage to the material or structural member investigated.

NDT methods are generally defined as those methods which do not impair the intended performance of an element or a structural member under test conditions. In regard to concrete, NDT techniques are intended to include also methods causing localised surface damage. The main advantage of these methods is that they can be performed on the concrete directly on site without the need to collect samples.

2.1. Destructive and Partially-Destructive Methods

In this Section, use of cores is discussed as the major destructive testing method for concrete. In regard to the use of partially-destructive methods, surface hardness methods are presented for the assessment of the quality of concrete. In addition to these, the penetration resistance method, the pull-out and pull-off and the break-off testing methods are discussed in regard to the evaluation of the strength of concrete.

2.1.1. Destructive Testing Methods

Coring is the most popular and established destructive way of testing concrete, as it allows visual inspections of the inner regions of a member to be coupled with strength estimations. Standards recommending procedures for cutting, testing and interpretation of results are available worldwide (e.g., BS EN 12504-1, 2009; ASTM C42, 2018); ACI 318, 2014).

160 The equipment usually employed for coring is a rotary cutting tool with diamond bits (Fig 1). To avoid drilling of distorted
161 or broken cores, the equipment must be firmly supported and braced against the concrete to prevent relative movements.
162 It is also necessary to provide a water supply in order to lubricate the cutter.
163 It is important to plan core location e size before testing. Core location is primarily linked to the basic purpose of the
164 testing. Regarding the core size, standards require a diameter of minimum three times the nominal maximum aggregate
165 size. In general, the accuracy decreases as the ratio of the aggregate size to the core diameter increases. 100 mm diameter
166 cores should not be used if the maximum aggregate size exceeds 25 mm, whereas 75 mm cores should be used preferably
167 for aggregate size of less than 20 mm. r.
168 Two basic classes of factors affecting measured core compressive strength can be mentioned. These are related to the
169 concrete characteristics and the testing variables. Regarding the concrete characteristics, the moisture condition of the
170 core affects the measured strength. Therefore, it is very important that the relative moisture conditions of the core and the
171 in-situ concrete are considered for the estimation of the actual concrete strengths. Voids in the core are also an important
172 factor capable to reduce the measured strength.
173 In regard to the testing variables, many different factors have been observed to affect the measured strength, i.e., i)
174 length/diameter ration of the core; ii) diameter of the core; iii) direction of drilling; iv) method of capping; v)
175 reinforcement.

176
177 **Fig. 1** A core cutting drill
178
179 ***2.1.2. Partially-Destructive Methods***
180 *Surface Hardness Methods*
181 Hardness is a key factor to test within the context of assessing the quality of concrete. Surface hardness methods can be
182 used in several application areas in order to assess the uniformity of concrete quality and compare the outcomes with

specific requirements. Furthermore, these methods can provide a reliable estimate of the concrete strength and resistance. First applications of measuring the surface hardness of a mass of concrete were recorded in the 1930s. They involved measurements of the size of indentation caused by a steel ball either fixed to a pendulum or a spring hammer, or fired from a standardised testing pistol. The height of rebound of the mass from the surface was then measured at a later stage. The purpose of these methods is not to establish a theoretical relationship between the values measured from any of these methods and the strength of concrete, but rather to define empirical relationships between test results and the quality of the surface layer.

The equipment is a rebound test hammer developed by the Swiss engineer Ernst Schmidt in the late 1940s (Fig. 2). The spring-controlled hammer mass slides on a plunger within a tubular housing. The plunger is pressed strongly and steadily against the concrete at right angles to its surface, until the spring-loaded mass is triggered from its locked position. After the impact, the scale index is read while the hammer is still in the test position. To avoid local variations of the values in the concrete due to irregularity of the surface, it is necessary to collect several readings for each test, typically nine spaced 25 mm from each other in an area not exceeding 300 mm^2 . Therefore, the surface must be smooth, clean and dry.

According to Bungey et al. (2003) several factors can affect the results. Some of these factors are related to the mix characteristics, i.e., i) cement type, ii) cement content, and iii) coarse aggregate type; whereas other factors relates to the member characteristics, i.e., i) mass, ii) compaction, iii) surface type, iv) age, v) surface carbonation, vi) moisture condition, vii) stress and temperature. Use of the rebound method is regulated by BS EN 12504-2 (BS EN 12504-2 2013) and ASTM C805 (ASTM C805 2018).

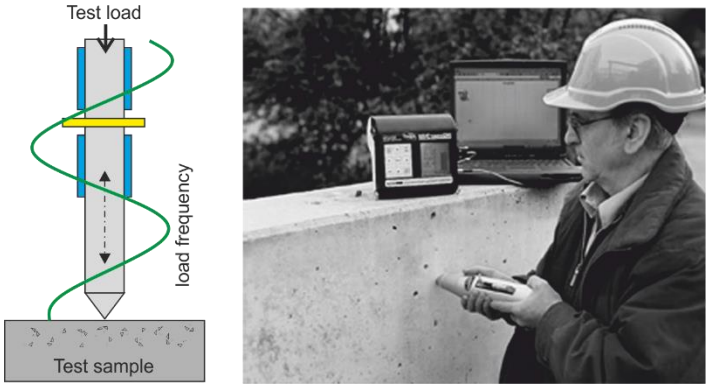

Fig. 2 The surface hardness test method (Bungey et al. 2006)

Penetration Resistance Testing

Penetration resistance testing (Fig. 3) is based on the principle that the depth of penetration is influenced by the strength of the concrete. A first application, known as the Windsor probe test, was developed in the US during the mid-1960s.

Although it is difficult to provide a theoretical relationship between the depth of penetration of the bolt and the concrete strength, robust empirical relationships can be found that are virtually not affected by the operator technique.

The test equipment consists in probes, generally of 6.35 mm in diameter and 79.5 mm in length, that can work alone or in groups of three. A system of triangular measuring plates is used to provide one averaged reading of the exposed length for the group of probes. The test procedure recommends to perform at least three tests and to provide an averaged outcome. In case the range of a group of three tests exceeds 5 mm, a further test should be performed and the extreme value discarded.

The principal physical limitation of this method is on the need of providing an adequate edge distance and a member thickness of at least twice the size of the anticipated penetration. Recommendations on the use of penetration resistance testing are given in BS 1881-207 (BS 1881-207 1992) and ASTM C803 (ASTM C803 2018).

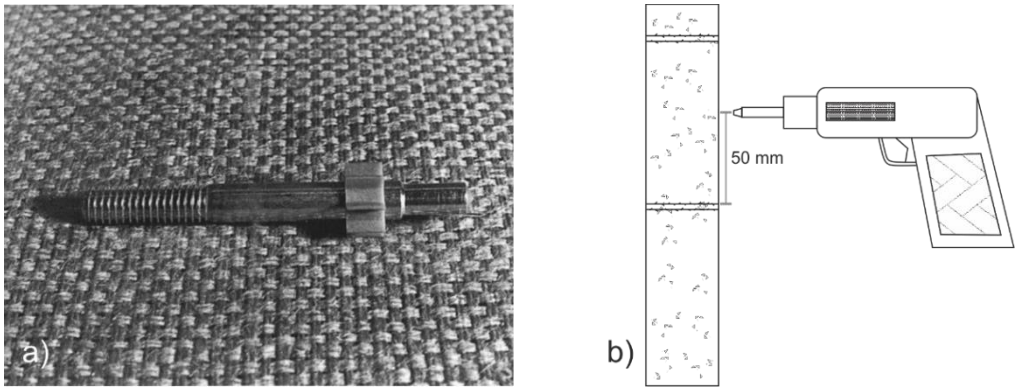

Fig. 3 Penetration resistance testing. **a** Penetration resistance test probe (Bungey et al. 2006), **b** layout of test procedure

Pull-Out and Pull-Off Testing Methods

Pull-out testing methods are based on measuring the force required to pull a bolt or other similar metal bars from a concrete surface. Tests fall into two classes, i.e., the cast-in and the drilled-hole methods. Cast-in methods involve an insert casted into the concrete, whereas drilled-hole methods provide an insert fixed into a hole which is drilled into the hardened concrete. In both cases, the value of the test is dependent on the ability to relate the pull-out force to the concrete strength. It has also been observed that this relationship is relatively independent from concrete mix features and curing history (Carino, 2004). An example of cast-in methods, i.e., the Lok-test, is illustrated in Fig. 4.

Pull-off methods (Fig. 5) have been developed to measure the in-situ tensile strength of concrete by applying a direct tensile force. Procedures are covered by BS 1881-207 (BS 1881-207 1992), ASTM C1583 (ASTM C1583 2013) (in-situ applications) and BS EN 1542 (BS EN 1542 1999) (laboratory applications on specimens) standards to assess the bond properties of repairing materials. These methods were developed initially in the early 1970s. Working principle provides

a disk to be glued to the concrete surface with an epoxy resin. The disk is jacked off to measure the force necessary to pull a piece of concrete away from the surface. A nominal tensile strength for the concrete is calculated based on the disk diameter. The compressive strength can be also calculated using a calibration chart appropriate to the concrete.

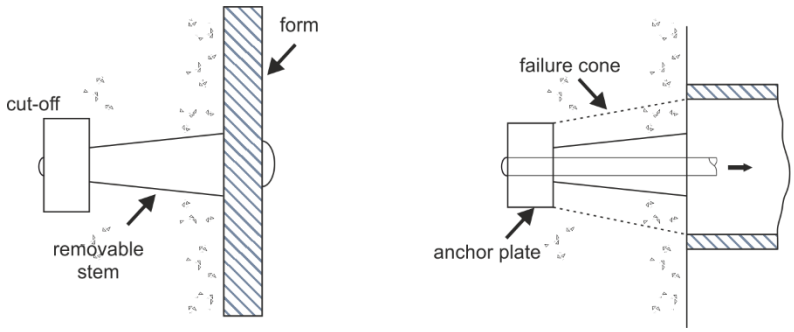

Fig. 4 Pull-out methods: the Lok-test insert

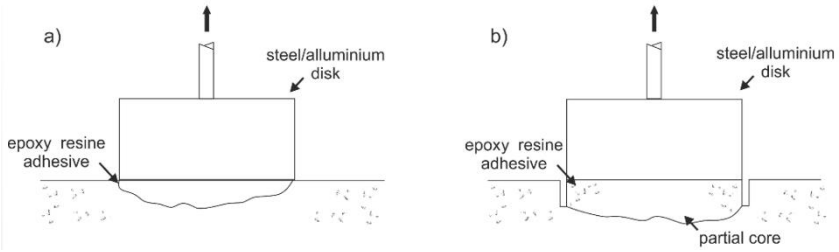

Fig. 5 The pull-off method. **a** Surface, **b** partially cored

Break-Off Testing Methods

The break-off technique has been developed following three different procedures. The procedure developed in Norway is known as "Norwegian method" (Ottosen, 1981) and it allows to determine directly the flexural strength in a plane parallel to and spaced from the concrete surface. The configuration of the test provides a tubular disposable form inserted into the fresh concrete. A transverse force is applied at the top surface in order to break the core left after the removal of the insert (Fig. 6). Specially developed portable equipment are used in order to exert hydraulically the breaking force. A linear correlation has been found between the break-off strength and the rupture modulus measured on prism specimens. The entire procedure and recommendations for this testing method are detailed in ASTM C1150 (ASTM C1150 2002). Another procedure known as the Stoll tork test (Stoll, 1985), was proposed later on in order to improve upon the variability of the existing similar techniques and to allow for testing at deeper depths than the pull-out, the pull-off and the penetration resistance methods. Accuracy of this testing method is comparable with that of the major partially-destructive methods, with results based on the average of at least three tests. The main value of the method is in the pre-planned monitoring of

the internal in-situ strength development, although further investigations are still required to foster a commercial use of the method.

A further test procedure for precast concrete quality control purposes has been used in the former Soviet Union, as discussed by Leshchinsky et al. (1990). However, this technique has not become an established international method for testing.

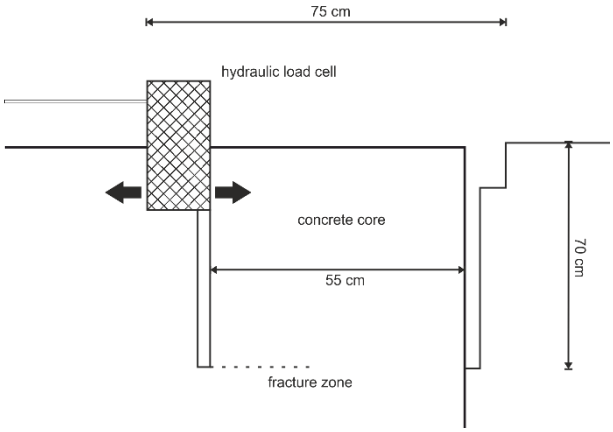

Fig. 6 The break-off method

2.2. Non-Destructive Methods

Several applications of NDT methods to concrete and reinforced concrete materials and structures can be found in the literature. Although research in this subject area is continuously in progress and use has not become established for many of these methods, promising results have been achieved to date. Table 3 reports an overview of the main NDT techniques used for concrete and reinforced concrete investigation purposes, highlighting their main advantages, limitations, areas of future research, and potential future challenges and prospects.

Table 3 Main NDT methods for investigation of concrete and reinforced concrete materials and structures

Method	Standard/Guideline	Characteristic	Theoretical frequency range	Application	Advantage	Limitation	Future research challenge and prospect
Sonic	• ASTM C597-16 (2016)	• Contact • Partially-destructive	500 Hz ÷ 10 KHz	• Evaluation of delamination (McCann and Forde, 2001) • Voids detection (Fegen et al., 1979) • Assessment of material uniformity (McCann and Forde, 2001; Guida et al., 2012) • Assessment of the average compressive strength of structures/materials (McCann and Forde, 2001)	• Reliability of results (McCann and Forde, 2001) • High-resolution imaging (Hollema and Olson, 2003) • Suitability for outdoor surveys (McCann and Forde, 2001) • Useful information on major structural elements (Guida et al., 2012)	• Invasiveness if electrical probes are needed (ACI 228.2R-13, 2013) • Complexity of result interpretation (McCann and Forde, 2001; ACI 228.2R-13, 2013) • High signal attenuation for high-resolution imaging (McCann and Forde, 2001) • Time-consuming data collection (ACI 228.2R-13, 2013) • Moderately high costs (McCann and Forde, 2001)	• Development of more user-friendly devices for data acquisition • Use of an array of transducers to limit data acquisition time

Ultrasonic	• ASTM C597-16 (2016) • ASTM D6760-16 (2016) • BS EN 12504 (2004) •	• Contact • Partially-destructive	20 ÷ 200 KHz	• Reinforcement detection (Pucinotti et al, 2007) • Location of a variety of defects within concrete elements (e.g., delaminations, voids, honey-combing) (ACI 228.2R-13, 2013) • Thickness evaluation of structural elements (ACI 228.2R-13, 2013) • Assessment of the relative condition or uniformity of concrete (ACI 228.2R-13, 2013)	• Portable equipment is available (ACI 228.2R-13, 2013) • Relatively easy to use (ACI 228.2R-13, 2013) • High speed of tests (Bungey et al., 2006) • Reliability of results (Bungey et al., 2006)	• No information on major elements (Bungey et al., 2006) • Applicable to limited member thickness (ACI 228.2R-13, 2013) • Experienced operators required (ACI 228.2R-13, 2013)	• Possibility to reduce signal attenuation effects
GPR	• ASTM D4748-15 (2015) • ASTM D6432-11 (2011) • ASTM D6087-08e1 (2015)	• Contact/Non-contact • Fully non-destructive	500 MHz ÷ 2.5 GHz	• Defect and decay detection (Wang et al., 2011; Martino et al., 2014; Miramini et al. 2018) • Location of rebars (Alvarez et al., 2017; Kien et al., 2018; Lachowicz and Rucka, 2018) • Estimation of rebar size (Utsi and Utsi, 2004; Chang et al., 2009; Zhou et al., 2018; Giannakis et al., 2019) • Measurement of dielectric properties (Louzli et al., 2002; Laurens et al., 2005; Sbartai et al., 2009b) • Industrial quality control (Wiwatrojanagul et al., 2017; Burgey et al., 2003)	• Totally non-destructive (Zhou et al., 2018) • Portable equipment (Daniels, 2004) • Use of different frequencies for different types of targets (Bungey et al., 2006) • Real-time continuous displaying of collected results (Miramini et al. 2018) • Rapid investigations of large areas (Bungey et al., 2003) • Very sensitive to presence of embedded metal objects (ACI 228.2R-13, 2013) • Sensitive to the presence of moisture and chlorides (ACI 228.2R-13, 2013)	• Skills required to interpret data (Burgey et al., 2003) • Congested reinforcement can prevent penetration beyond the reinforcement (ACI 228.2R-13, 2013) • Difficulty in detecting early-stage decay (Burgey et al., 2003) • Cracks and delaminations not easy to detect unless moisture is present in the cracks or in the region of the delamination (ACI 228.2R-13, 2013) • Limited depth of penetration of pulses from high-resolution antennas (300 to 500 mm) (ACI 228.2R-13, 2013)	• Improving existing knowledge on the behaviour of the EM pulses through reinforced concrete structures • Use of higher central frequencies for detection of early decay • Development of real-time algorithms for concrete investigation
Microwaves	/	• Non-contact Fully non-destructive	250 MHz ÷ 300 GHz	• Concrete decay (Patriarca et al., 2011; Hashemi, 2016) • Moisture distribution (Rhim and Buyukozturk, 1998; Bouichou et al., 2018)	• Small size of the antennas (Hashemi, 2016) • High-resolution measurements (Bouichou et al., 2018)	• Available hardwires not suitable for outdoor surveys (Hashemi, 2016) • Difficulty to identify the nature of decay (Hashemi, 2016)	• Better understanding of the physical properties of decays • Additional research required with computer analysis and sensor technology • Need for more quantitative results
Infrared Thermography	• ASTM D4788-03, (2013)	• Non-contact • Fully non-destructive	3 THz ÷ 428 THz	• Voids and delamination detection (McCann and Forde, 2001) • Defect evaluation (Holt and Eales, 1987) • Assessment of concrete moisture conditions (Grinzato et al., 2011) • Construction details (Titman, 2001) • Detection of reinforcing bars (Maierhofer et al., 2006)	• Reliability of results (Stanley and Balendran, 1995) • Suitability for rapid assessment of large or high-rise buildings (Stanley and Balendran, 1995) • Remote use without direct coupling with structure/material (ACI 228.2R-13, 2013) • Good overview of decay areas in the survey region (ACI 228.2R-13, 2013) • Real-time displaying of collected results (Rocha et al., 2019)	• Variations in the test response with varying environmental conditions (McCann and Forde, 2001; ACI 228.2R-13, 2013) • Limitations in detecting deep defects (Stanley and Balendran, 1995; ACI 228.2R-13, 2013) • Difficulty in decay detection for low-quality concrete (Rocha et al., 2019) • Expensive equipment (ACI 228.2R-13, 2013) • Experienced operator required (ACI 228.2R-13, 2013)	• Investigation of deeper layers • Use of special filters to reduce the effects of variable environmental conditions
Radiography	• BS 1881-205:1986 (1986) • ASTM C1040 / C1040M-16a (2016)	• Contact • Fully non-destructive	1×10^4 THz ÷ 3×10^6 THz (X-rays) 3×10^6 THz ÷ 3×10^{10} THz (ϒ-rays)	• Providing view of the internal structure of the test object (Mishin, 1997; ACI 228.2R-13, 2013) • Use of image plates to extract more information about the internal structure of the test object (ACI 228.2R-13, 2013) • Checking of reinforced bars (Mitchell, 1991) • Use of portable iridium-192 (Ir) sources in holes drilled in concrete to provide tomography of reinforcement in large columns and beams (ACI 228.2R-13, 2013)	• Equipment can be turned off when not in use (X-rays) (ACI 228.2R-13, 2013) • Equipment reasonably portable and cost-effective (ϒ-rays) (ACI 228.2R-13, 2013) • Minimal operator skills required for data collection (ϒ-rays) (ACI 228.2R-13, 2013) • Reliability of results for large datasets (Bungey et al., 2006)	• Safety concerns due to the emission of hazardous radiations (ACI 228.2R-13, 2013) • Operators must be licensed and highly skilled. • Bulky and expensive equipment (X-rays) (Bungey et al., 2006; ACI 228.2R-13, 2013) • ϒ-ray penetration limited to 20 in. (500 mm) within concrete materials (ACI 228.2R-13, 2013) • Access to opposing faces required (ACI 228.2R-13, 2013) • Large differences more readily detected than small differences (Mishin, 1997) • Difficulty to identify cracks perpendicular to the radiation beam (ACI 228.2R-13, 2013)	• Additional research required to deal with large data samples

In regard to the existing standards for use of NDT techniques in concrete investigations, four classes of NDT methods are presented in this Section which have been sorted by the main inspection task, i.e., (1) ultrasonic pulse velocity methods for concrete quality control purposes; (2) durability tests for concrete decay assessment due to weathering action and chemical attack; (3) performance and integrity tests and (4) load testing methods.

2.2.1. Quality Control Tests: Ultrasonic Pulse Velocity Methods

The first application of pulse velocity methods in concrete dates back to the mid-1940s, USA. Methods were considered reliable in view of a strong dependence of the velocity upon the elastic properties of the material. A few years later, a repetitive mechanical pulse equipment was developed in France to overcome measurement problems. Nowadays, modern ultrasonic methods, employing pulses in a frequency range of 20–150 kHz, are the most diffused.

In terms of working principles, a source pulse is transmitted to the concrete surface and a recorded pulse is received and amplified. This allows to measure the time elapsed with an accuracy of ±1%. The wave velocity within the medium depends on the elastic properties and the mass of the medium. Hence, it is possible to assess the medium elastic properties if its mass and the wave propagation velocity are known (Trtnik et al., 2009).

The ultrasonic pulse velocity method can be used in both laboratory (Popovics et al., 1990; Bogas et al., 2012) and on-site testing conditions (Lee et al., 2004). Main applications in the laboratory environment consist in the monitoring of material design characteristics and structural behaviour, e.g., strength development or deterioration in specimens subject to varying curing conditions or aggressive environments. Testing on the site allows to (i) measure the material uniformity (ii), detect cracking, (iii) have an estimation of the strength of the concrete, (iv) assess concrete deterioration (v) measure the thickness of concrete layers and (vi) to estimate the material elastic modulus.

Testing in the vicinity of reinforcement should be avoided as considerable uncertainty is introduced by the dominant influence of steel over concrete. The case of reinforcement parallel to the pulse path (Fig. 7) and transverse to the pulse path should be considered in order to apply corrections to the actual value of velocity of propagation in the concrete. Specifications on the use of the ultrasonic pulse velocity method are given in BS EN 12504 (BS EN 12504 2004) and ASTM C597 (ASTM C597 2016).

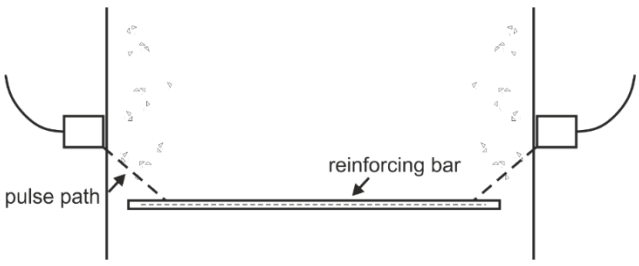

Fig. 7 The ultrasonic pulse velocity method for reinforcing bars: case of reinforcement parallel to the pulse path

2.2.2. Durability Tests

Durability tests aim to assess the material characteristics affecting this particular feature as well as to identify the problem source. Deterioration of structural concrete may be due either to the action of chemical and weathering agents, and corrosion of embedded reinforcement steel is an element of major concern. Within this framework, durability tests involve different types of assessment such as the corrosion detection, moisture measurements and the absorption and permeability tests.

Corrosion of Reinforcement

Corrosion of reinforcement bars is an electro-chemical process that requires the contribution of moisture and oxygen. This process is often acknowledged as the major cause of decay in concrete structures. This occurrence may lead to a structural weakness due to the loss of the steel cross-section, surface staining and cracking or spalling. In some instances, internal delamination may also occur and, to this effect, EM methods are nowadays the most used for purpose. In this regard, battery-operated devices known as covermeters are employed (**BS 1881-204, 1988**). The fundamental working principle relies on the fact that steel affects the field of an electromagnet (i.e., an iron-cored inductor). An alternating current is passed through one of the coils, while the current induced in the others is amplified and measured. The reliability of this technique depends on factors affecting the magnetic field within the metre range. Among these, the presence of multiple reinforcing bars, laps or transverse steel, metal tie wires, variations in the iron content of the cement and use of aggregates with magnetic properties are worthy of mention.

More recently, the half-cell or rest-potential measurement method has been applied to assess areas of potential reinforcement corrosion. The method measures the potential of embedded reinforcing steel relative to a reference half-cell placed on the concrete surface (Fig. 8) (ASTM C876, 2009). It is also worth to mention that the half-cell potential method can be used in combination with resistivity measurements. The resistivity method works upon the ability of corrosion currents to flow through the concrete that can be assessed in terms of the electrolytic resistivity of the material.

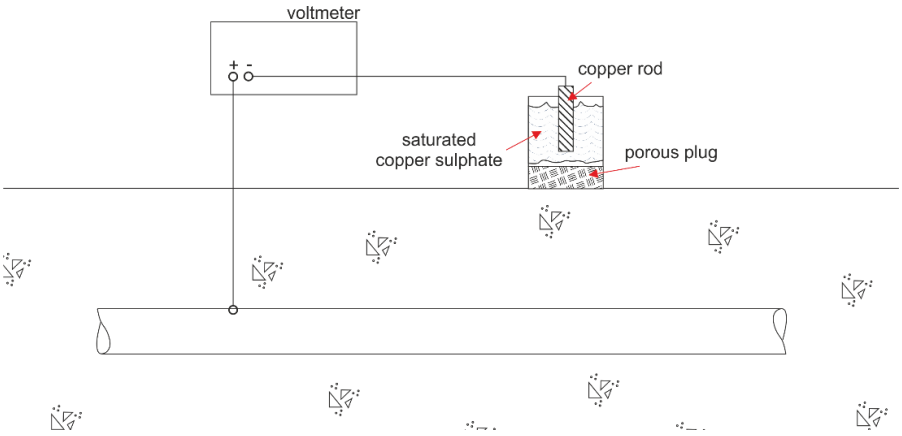

Fig. 8 Measurement framework for the reinforcement potential method

Moisture Detection

Electrical methods (Fig. 9) are the most widespread within this assessment area as electrical resistivity measurements are highly sensitive to moisture. The dielectric properties of concrete are highly affected by the content of water, and factors such as the dielectric permittivity of the material and the dissipation factor can provide robust indications on moisture presence. It is known that the properties of a capacitor formed by two parallel conductive plates depend upon the characteristics of the separating medium. To this effect, the ratio between capacitances of the same plates when separated by the tested medium and by a vacuum identifies the dielectric permittivity.

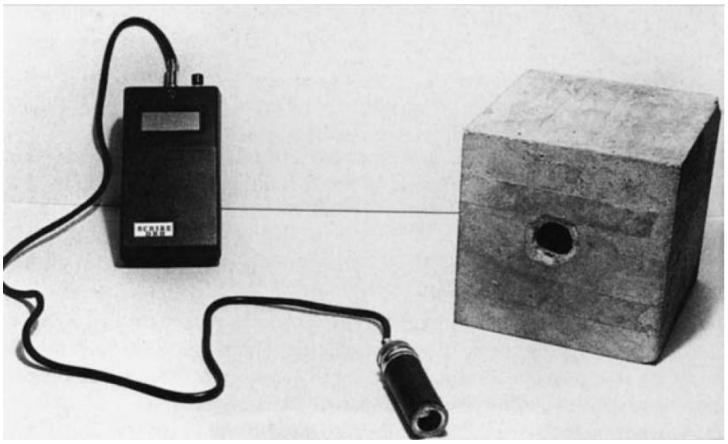

Fig. 9 A humidity meter for detection of moisture (Bungey et al., 2006)

Absorption and Permeability Tests

The absorption and permeability tests are relevant for the assessment of concrete in water retaining structures or watertight basements, as well as to have an estimation of the material durability. Among the existing methods within this assessment area, the most utilised is the initial surface absorption method (Fig. 10) (BS 1881-208, 1996). Levitt (1969) has discussed the theory and the application of this technique and further analytical studies (Wilson et al., 1998) present the working mechanisms in detail.

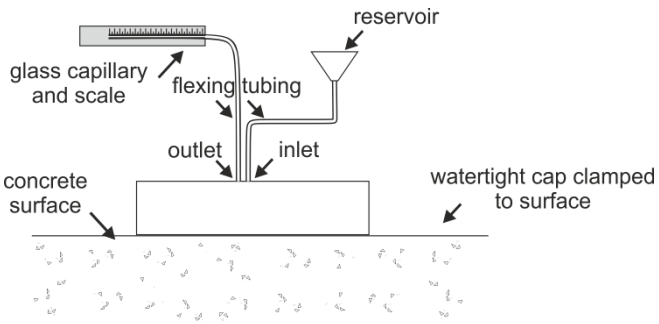

Fig. 10 The initial surface absorption test

2.2.3. Performance and Integrity Tests

Infrared Thermography

The infrared thermography test is based on the analysis of images collected using a special camera (Fig. 11) during the cooling of a heated structure. Use of this technique has many potential advantages over physical methods for the detection of structural delamination, as it was discussed by Manning and Holt (1980). The detection of laminations or voids by infrared thermography is based on the difference in surface temperature between sound and unsound concrete under certain atmospheric conditions. First unsuccessful attempts were performed with a camera held by an operator standing on a bridge deck. The limited field of view and the oblique alignment made this method as impracticable. Therefore, the technique was improved using an elevated mobile platform to scan the deck from a height of up to 20 m, provided that the surface temperature differentials were greater than 2°C.

Procedures for use of infrared thermography in the investigation of bridge deck delamination are given in ASTM D4788-03 (ASTM D4788-03, 2013). Other applications to concrete structures involve the assessment of concrete moisture conditions influencing thermal gradients, and the location of hidden voids, ducts and services. The infrared thermography technique has nowadays reached a level of sensitivity to temperature differences of ±0.1 °C and allows high-definition imaging and accurate temperature measurement.

Fig. 11 Infrared thermography apparatus (ACI 228.2R-13, 2013)

Ground-Penetrating Radar

The use of GPR systems for the investigation of concrete structures has increased over the last 20 years (Cantor, 1984). GPR working principles rely on the propagation of EM waves through the material, with the speed and attenuation of the signal being affected by its electrical properties. Since radar wave reflections occur at the interface between materials

with different dielectric properties, the back-reflected signal can be interpreted to provide an evaluation of the properties and the geometry of the subsurface. Within this context, a typical frequency range for applications to concrete is 500 MHz–2.5 GHz.

Three different approaches can be listed in regard to the use of GPR systems for the investigation of concrete structures: (1) frequency modulation with continuous frequency of the transmitted radar within a default frequency range; (2) synthetic pulses with varied frequency of the transmitted radar signal over a series of discontinuous steps; (3) impulse radar-based systems working with a series of discrete sinusoidal pulses within a specified broad-frequency band and a signal repetition rate of 50 kHz. A typical radar equipment configuration consists of an antenna in contact with the concrete surface to produce a diverging beam of radiation. An alternative to this is to use a focused beam horn antenna with an air gap of about 300 mm between the horn and the concrete surface. This latter technique is well-established and operational details are provided in ASTM D4748-15 (ASTM D4748, 2015). An overview of the equipment, the field procedures and the interpretation methods for the assessment of subsurface materials using GPR are provided in the ASTM D6432-11 standard (ASTM D6432-11, 2011). More specifically, on concrete, the ASTM D6087-08 standard (ASTM D6087-08, 2015) covers in detail a number of GPR procedures for the assessment of the concrete bridge deck overlaid conditions with asphaltic concrete wearing surfaces. Guidance is provided for identifying the concrete or rebar deterioration at or above the level of the top layer of reinforcing bars using GPR systems equipped with air-launched horn antennas or ground-coupled antennas of central frequencies of 1 GHz and greater.

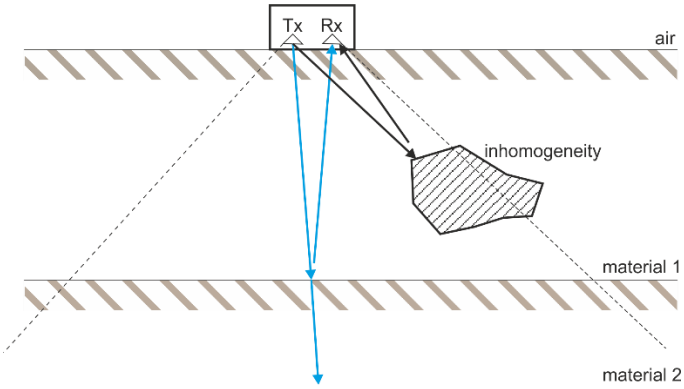

Fig. 12 Investigation of a subsurface anomaly using a GPR ground-coupled antenna system

2.2.4. Load Testing

Load testing may be necessary in case the strength of structural members cannot be adequately assessed using other available tests. Two classes of load tests can be primarily identified, i.e., the static tests (most common) and the dynamic tests, where variable loading are predominantly applied. An additional classification sorts load tests into non-destructive, generally carried out in-situ, and destructive, generally applied on members removed from a structure.

The principal aim of these tests is to prove satisfactory structural performance under the effects of an overload above the design working value. This is usually tested by measuring deflections sustained for a certain period of time under the action of the overload. In-situ load tests require a minimum age of the concrete of 56 days in order to be carried out. According to BS 8110 (BS 8110, 2003), loads must be added and removed incrementally, with the test load being applied twice minimum at a time interval of 1 hour between two consecutive ones. An example of load test for light roof purlins is shown in Fig. 13.

Reliability of in-situ load tests depends upon a number of key factors, such as a suitable preparatory work to avoid potential restraints, the accuracy provided in the application of the load, the provision of an accurate datum for deflection measurement and a careful allowance for temperature effects. Compliance of these requirements provides a reliable indication of the behaviour of the member or the structure under test for short-term tests.

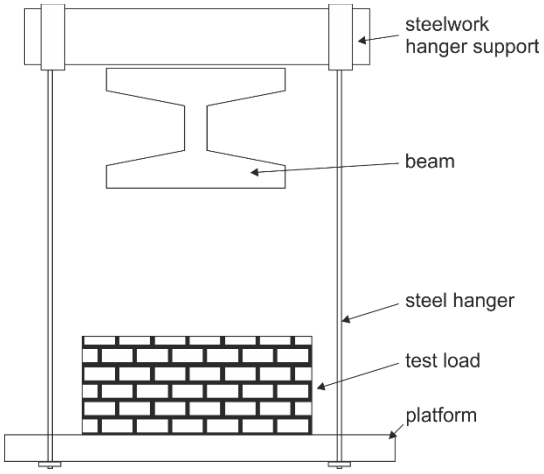

Fig. 13 The load test for light roof purlins

3. THE GPR TECHNOLOGY

3.1. Theoretical Background

GPR principles feed into the EM theory where the physics of the EM field propagation is described by the Maxwell's equations and material properties are quantified by constitutive relationships. As a combination of these two factors, the GPR signal is the output that provides information on the subsurface properties and configuration.

The propagation of the EM waves depends on the three main EM properties of the host material (Benedetto et al., 2017), i.e., the dielectric permittivity ε, the electric conductivity σ and the magnetic permeability μ.

The dielectric permittivity and the electric conductivity are strictly related to the EM wave features. ε affects the wave velocity, and σ controls the wave attenuation. On the contrary, the magnetic permeability μ does not relate with the propagation of the wave for all the non-magnetic materials, as it is equal to the free-space magnetic permeability μ_0.

On the other hand, the main factors affecting the penetration depth are the frequency of the emitted signal (for structural inspections, antennas with central frequencies above 1 GHz are used) and the type of material investigated.

From a theoretical point of view, the physics of EM fields is described by the Maxwell's equations as follows:

$$\nabla \times \vec{E} = -\frac{\partial (\vec{B})}{\partial t} \quad (1)$$

$$\nabla \times \vec{H} = \vec{J} + \frac{\partial (\vec{D})}{\partial t} \quad (2)$$

$$\nabla \cdot \vec{D} = q \quad (3)$$

$$\nabla \cdot \vec{B} = 0 \quad (4)$$

where:

$\vec{E}$= strength vector of the electric field (V m^{-1}); q= electric charge density (C m^{-3}); $\vec{B}$= density vector of the magnetic flux (T); $\vec{J}$= density vector of the electric current (A m^{-2}); $\vec{D}$= electric displacement vector (C m^{-2}); t= time (s); $\vec{H}$= intensity vector of the magnetic field (A m^{-1}).

Material properties are instead quantified by the following constitutive relationships:

$$\vec{J} = \sigma \vec{E} \quad (5)$$

$$\vec{D} = \varepsilon \vec{E} \quad (6)$$

$$\vec{B} = \mu \vec{H} \quad (7)$$

Combination of the EM fields' theory and the material properties allows to describe comprehensively a GPR signal.

3.2. Working Principles

3.2.1. Overview

GPR is a geophysical inspection technique used for the non-destructive investigation of the subsurface. Fig. 14 represents a GPR output from a survey layout typical of a reinforced structure. An EM wave is emitted towards the surface by a radar with a fixed central frequency using one or more antennas. The signal is then received as a function of the material properties and characteristics of the receiving antenna. A GPR signal is characterised by a series of peaks with amplitude values dependent on three main factors, i.e. the nature of the reflector, the nature of the travelled medium and the curve of the applied amplification (Noon, 1995). Typically, three visualisation modes can be listed for a GPR signal that provide three different levels of information: i) an A-scan, i.e. a single radar trace along the depth axis; ii) a B-scan, i.e. a set of sequential single radar traces collected along a specific scanning direction; and iii) a C-scan, i.e. a set of B-scans extrapolated at a certain spacing along the depth axis (Benedetto et al., 2017).

Various information can be collected with GPR, such as the two-way travel time distance between reflection peaks at layer interfaces/target positions (e.g. rebars), the amplitude and the phase of a signal. To this effect, locating rebars and estimating cover thickness are among the major applications of GPR to reinforced concrete structures.

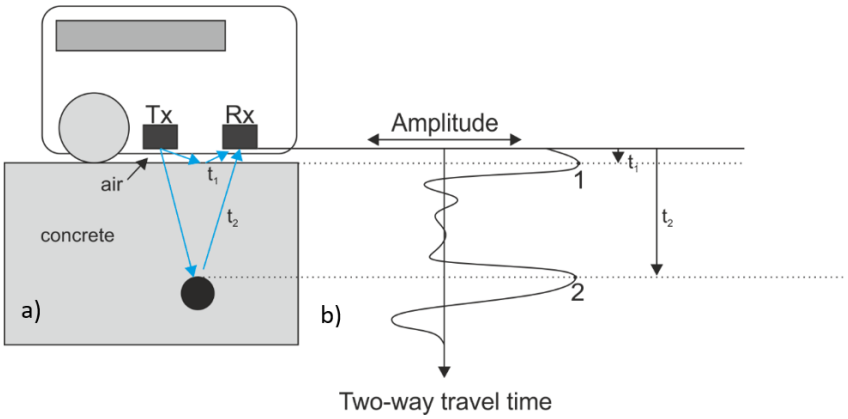

Fig. 14 a Layout of a survey on a reinforced concrete structure using a ground-coupled GPR system, **b** corresponding GPR signal output

3.2.2. Configuration of the Antennas

A GPR system is configured as mono-static when a unique antenna operates as both transmitter and receiver, and bi-static in case of separated transmitter and receiver. In addition, GPR systems can be sorted as ground-coupled or air-coupled, as a function of the type of antennas. Ground-coupled antenna systems work in direct contact with the surface and allow for a higher penetration depth. A typical frequency range for these systems is from 80 MHz to 2000 MHz. Air-coupled antennas work attached to an inspection vehicle and allow for a faster acquisition. The radar apparatus are usually set up at 0.15 m÷0.50 m above the surface and the central frequency ranges typically from 1000 MHz to 2000 MHz.

For concrete structure inspections, ground-coupled antennas with central frequencies above 1 GHz are usually employed to provide a trade-off between accuracy and depth of inspection (Hugenschmidt, 2002; Burgey, 2004).

3.3. GPR Applications in Reinforced Concrete Materials and Structures

GPR is a fundamental method for quality control and routine inspections of reinforced concrete in civil engineering infrastructures (Wiwatrojanagul et al., 2017). The suitability of GPR is related to the presence of concrete (low-conductive material) and rebars (high-conductive materials), which allow for effective detection in the composite material. The very first application of a radar system in detecting metal objects dates back to 1904 (Ulricksen, 1982), whereas the use of GPR in structures started to gain momentum in 1980s (Forde, 2004). Nowadays, GPR is used for many applications in

472 the area of reinforced concrete materials and structures, although the location of reinforcing bars is one of the most
473 widespread (Pucinotti and De Lorenzo, 2006).
474 The main applications in the literature within this subject area are: i) the location of reinforcing bars, ii) the detection of
475 rebar corrosion, iii) the estimation of the rebar size, iv) the evaluation of the concrete cover, v) the structural detailing of
476 anchorages and joints in major structures/infrastructures, and v) the assessment of concrete characteristics (i.e. uniformity,
477 voids, cracks, strength and durability) by analysing the material dielectric properties.
478 In regard to the assessment of reinforcing bars, damage to these elements is the most serious source of structural decay in
479 concrete structures, with many economic implications leading to repair or, eventually, replacement of the main structural
480 element.
481 Locating reinforcing bars is of primary importance in both quality control inspections of new structures and infrastructures
482 as well as in the structural detailing of existing ones (Benedetto et al., 2012; Stryk et al., 2013; Stryk et al. 2018). In
483 addition, it is known that corrosion of rebars, usually due to moisture ingress and chloride ion exposure (Shi et al. 2012),
484 can cause subsurface cracking and spalling of the concrete cover. This occurrence promotes water and chloride
485 infiltration, which in turn can generate delamination around the reinforcing bars. Within this framework, the GPR
486 technique has proven its viability to detect corrosion in rebars due to signal attenuation effects from moisture and chloride
487 ingress (Laurens et al., 2000; Kim et al., 2003; Hugenschmidt and Loser, 2008). Estimating the size of rebars is another
488 topic of major interest. Although several promising approaches and numerical-based applications have been reported in
489 the literature, further research is still required in order to make GPR a reliable and established technique for the purpose
490 (Utsi and Utsi, 2004; Zanzi, 2012; Giannakis et al., 2019). GPR has been extensively used for the assessment of concrete
491 covers as both a self-reliant equipment (Klysz et al., 2004; Al-Qadi and Lahouar, 2005; Hasan and Yazdani, 2014) and in
492 combination with other NDT methods (Dèrobert et al., 2008).
493 The assessment and the health monitoring of major reinforced-concrete structures and infrastructures is another important
494 application area for the GPR techniques. To this effect, an early diagnosis of decay at key areas, such as anchorages in
495 building foundations and pre-stressed beams, joints in bridge decks (Benedetto et al., 2012) and tunnel linings (Alani and
496 Tosti, 2018), can limit the risk of known consequences such as accidents, closures and ultimately devastation. The
497 assessment of concrete characteristics is another research area of major development. In this regard, the detection of
498 cracks (Benedetto, 2013) and voids (Cassidy et al., 2011) as well as the assessment of concrete strength and durability
499 features (Sbartai et al., 2009; Villain et al., 2010) have been widely investigated in the literature.
500

501 **4. RESEARCH METHODS ON THE USE OF GPR IN REINFORCED CONCRETE STRUCTURES: AN**
502 **HISTORICAL REVIEW**

An historical review of research within the context of the applications of GPR to reinforced concrete structures is given in this Section. Discussed research methods are sorted according to the scale of investigation (i.e. laboratory and numerical environments, and real-life scales of investigation) and the main application areas identified above. A chronological overview of the main research findings achieved within every application area is therefore reported. Overall, it was observed that not all the application areas have been covered at both the laboratory and the real-life scale of investigation. A lack of case studies has been noticed in certain areas in the case of applications to real-life scenarios. This could be due to practical constraints preventing full control of the boundary conditions, as well as to clear difficulties in validating research outcomes by a destructive way of practice. On the contrary, these factors become easier to control and analyse in a laboratory environment. It was also noticed that the use of pulsed GPR systems was preferable to the use of stepped-frequency continuous-wave (SFCW) radar systems. This is likely due to the higher cost of electronics, an overall major complexity in data processing (i.e. high computational requirements) and a lack of dedicated commercial software (Gagarin and Mekemson, 2016).

4.1. Laboratory-scale Investigations and Numerical Developments

4.1.1. *Location of Reinforcing Bars*

The location of reinforced bars has had more applications in real-life scenarios rather than in a laboratory environment. This may be related to the fact that this operation is relatively practical, as it requires the identification of the apex of the hyperbolic target reflections. Migration processing can help to estimate the actual propagation velocity of the EM wave through the concrete cover and, therefore, to precisely locate the rebar position.

Extensive research was carried out by Bungey et al. (1993). Tests were developed in a laboratory to identify the position of reinforcing bars using a 1 GHz GPR antenna system. The effects of round steel reinforcing bars with diameters between 6 and 32 mm have been analysed at depths of up to 280 mm below the surface of the concrete. This has been facilitated by the use of a timber-analogue simulation tank in which the dielectric and conductivity properties of the concrete were replicated using an oil-water emulsion. In excess of 250 different configurations were analysed and results were validated by way of comparison with a number of concrete samples and by site trials on members of known construction details. More recently, Zhou et al. (2018) used GPR in combination with the electromagnetic induction (EMI) method to accurately locate reinforcing bars. The authors utilised a number of four casted concrete specimens with 11 embedded steel rebars, proving a correct estimation of the rebar size for 10 out of the 11 rebars.

In regard to the use of numerical modelling for rebar location, Alvarez et al. (2017) used the gprMax numerical simulator tool (Giannopoulos, 2005) to generate realistic, big data sets of different concrete covers for training-driven machine learning approaches. Although the approach was tested against a concrete-analogue scenario made of a sand-based

534 mixture, the authors found the simulation package to be suitable for generating realistic outputs. Lachowicz and Rucka
535 (2018) presented numerical and experimental investigations to localise reinforcing bars using GPR methodology. In more
536 detail, a new approach for the numerical modelling of GPR in complex reinforced concrete structures with the use of a 3-
537 D finite-difference time-domain (FDTD) model was presented. Comparison between simulated results and real scans has
538 proven the viability of the proposed model to work on a complex reinforcement system. More recently, Kien et al. (2018)
539 presented an automated rebar-picking algorithm for GPR data of concrete bridge decks with the aim of identifying and
540 locating rebars. The algorithm is based on the Limited and Simplified Hyperbolic Summation (LSHS) technique where
541 the width of migration is limited and a counter is used to check if a hyperbolic signature exists in a sub-region of the GPR
542 image. The application of the algorithm to GPR datawas promising and in a good agreement with the existing techniques
543 based on manual rebar picking.
544
545 **4.1.2.** ***Detection of Rebar Corrosion***
546 The interest of using GPR for detection of steel bar corrosion is growing nowadays. An early diagnosis can support
547 decision-makers to prevent the spreading of damage throughout the structure and to containing maintenance costs. To
548 this effect, research efforts have been directed towards the identification of wet areas nearby the rebars, where the
549 corrosion process is most likely to be found. It was observed that most of the research methods developed for this
550 particular application area have been performed in a laboratory environment. This is due to more favourable conditions
551 in controlling the ingress of corrosion agents and, hence, to identify areas of potential decay. It was also noticed that
552 results obtained from a number of these research studies were implemented on the site at a later stage and combined with
553 conventional methods.
554 Narayanan et al. (1998) analysed the statistical variance of rebar reflectivity to detect corrosion using 400 MHz and 900
555 MHz antenna frequencies. Results have proven a better agreement of the 900 MHz central frequency with the ground-
556 truth data. A subsequent research was carried out to identify a threshold between healthy and corroded rebars (Narayanan
557 et al., 2003). The variance simulations supported to identify the reflectivity of the corroded rebar. Laurens et al. (2000)
558 and Barnes et al. (2008) observed that lower relative reflection amplitudes and larger travel times of the GPR signal are
559 an indication of a high corrosion and deterioration of rebars. In this regard, it was observed that moisture and chlorides
560 dissolved within the concrete attenuate the signal back-reflected from the rebars. This occurrence decreases the wave
561 propagation velocity and increases the arrival times of reflection peaks. A relationship between the amplitude data of the
562 reflections from rebars and the corrosion process was confirmed by Hubbard et al. (2003). The authors used GPR and
563 electrical impedance to analyse rebar corrosion in a reinforced concrete block. Research outcomes were validated by
564 visual examination of the reinforcing bar corrosion state via destructive analysis of the experimental block. Results have

proven the viability of GPR in providing indication of alterations at the interface of the reinforcing bar surface and the surrounding concrete. GPR was also proven to provide a higher spatial resolution than the electrical impedance. These outcomes were valuable indications that GPR can be used for an early detection of corrosion-related processes of decay. More recently, Raju et al (2018) employed a hand-held ground-coupled GPR system equipped with an antenna frequency of 2.6 GHz in order to assess reinforcing bar corrosion. A saltwater solution was used to control the corrosion process in a laboratory environment. The authors related the corrosion with the maximum reflected amplitude obtained from the GPR scans. Results have proven that the reinforcing bar corrosion mass loss was higher for longer corrosion periods, larger reinforcing bar size, and shorter covers. It was also noticed that the GPR amplitude values increased proportionally with the corrosion activity.

Few research is reported on the use of the numerical simulation for detection of corroded areas. This is due to the complexity in the physics and the chemistry of the process as well as to the effect of the corrosion on the surrounding construction elements. This complex scenario involves multiple scatterings of the signal from the rebar-concrete system and the corroded areas in rebars and/or other defects in the concrete. Bachiri et al. (2018) developed a numerical model of a bridge deck and analysed scenarios of healthy and corroded rebars. Results have shown that a proper selection of the working frequency value is crucial to increase the survey resolution and the likelihood to detect corrosion. The authors claimed that an experimental validation is however required to confirm the outcomes of the simulation.

4.1.3. *Estimation of Rebar Size*

Estimation of rebar size is a topical and very challenging application area, and research is still in progress to provide viable and comprehensive methodologies. In this regard, it was observed that all the methods have been developed in a laboratory environment, proving that the research applicability in this area is at an early stage of development. A common approach to this problem is to use numerical modelling and to validate the observations with experimental activities carried out on samples in a laboratory environment.

Utsi and Utsi (2004) proposed a three-dimensional numerical model assuming one metal bar for a range of diameters and cover depths. Frequencies of 2 GHz and 4 GHz were used for simulation purposes. Results showed that the amplitudes of the signals back-reflected from the rebars are proportional to their size and the frequency is inversely proportional to the depth of the investigation. These results were compared with measurements of rebars placed at known distances below a 4 GHz GPR system with free space in between. According to the authors, an accuracy of about 20% can be reached in estimating rebar size. Another issue was encountered in case of a rebar spacing lower than the wavelength of the used GPR, as this may compromise the data collection for rebar size estimation purposes.

Chang et al. (2009) reported a physical model based on the use of digital image GPR for measuring the radius of reinforcing steel bars in concrete. To this purpose, several specimen of 120 × 60 cm dimensions were produced using rebars of 1 cm and 1.6 cm radii. Concrete cover depths varied from 4 to 10 cm. GPR radargrams were subject to a series of digital image processing stages, followed by different power reflectivity within the energy zone during the motion of the GPR antenna along the reinforced concrete surface. Power reflectivity for vertically-oriented migration traces was generated. The authors argued that the distance between a variant power reflectivity and the long dimension radius of an energy footprint must be considered for the evaluation of a rebar radius. Results indicate an error for the estimation comprised within 7%. Zanzi and Arosio (2012) used a 1 GHz and a 2 GHz GPR systems on two concrete specimen of 40 cm width, heights of 15 and 18 cm, and lengths of 105 and 110 cm, respectively. Rebar diameters from 6 to 40 mm, spaced 20 cm each other were analysed. The experimental scenario was replicated using numerical simulations. The authors identified the interference of the background signal with the wavelets scattered by the rebars as the main issue to address in order to achieve quality information. Near-field and bandwidth-related issues seemed to be of less priority in generating potential misfits between theoretical and real measurements. A set of three antennas with nominal frequencies in the 600-MHz ÷ 2000 MHz range were indicated as a good trade-off for detection of rebars with diameters up to 40 mm. However, a cross-check of the results in a real-life scenario was suggested by the authors in order to consider the impact of the concrete cover and the quality upon the reliability of the rebar size estimation. To this effect, use of a high-frequency dual-polarised antenna system was suggested along with a survey methodology aimed at collecting a robust statistical population of rebar points.

In view of the high density distribution of rebars in a reinforced concrete structure, finding comprehensive and fast inspection algorithms and methodologies for detection of rebar corrosion has been identified as a major research subject area. In this regard, Shaw et al. (2003) developed a neural network approach to automate the estimation of the rebar size diameter from data collected with the transducer axis parallel and orthogonal to the bar. To this effect, an emulsion analogue tank simulating the properties of concrete, was used to produce training data and the resulting neural network was then tested on actual reinforced concrete slabs. Results have proven a good estimate of the rebar size for both high and low concrete covers. More recently, Mechbal and Khamlichi (2017), proposed a method for the estimation of the rebar radius by data processing of B-scan radargrams collected orthogonally to the rebar axis. The approach relies on use of the hyperbola fitting method and the information from diffracted amplitudes. Hyperbola fitting has proven to be extremely sensitive to noise affecting raw data points. It was also demonstrated that use of extra information in terms of maximum diffracted amplitudes enhanced the accuracy of rebar radius estimation.

Giannakis et al. (2019) proposed a near-real-time forward modelling approach for GPR based on a machine learning (ML) architecture. The method was used to determine location and size of reinforcement bars in concrete. The authors have

used simulations to train a ML-based forward solver and validated the approach with real data collected on a concrete specimen. A 1.5-GHz antenna frequency was used to investigate a rebar size range between 4 and 50 mm and a cover depth varying from 0 to 300 mm. Results have proven a good level of accuracy in the estimation of the target parameters, including a maximum error in the estimation of the rebar size of 6 mm. The authors emphasised on the viability of using a full-waveform inversion approach in near-real-time computation conditions for application to more complex scenarios.

4.1.4. The Evaluation of the Concrete Cover

The evaluation of the concrete cover has found more applications in real-life scenarios rather than in a laboratory environment. Within this framework, major laboratory-based research was carried out by Dérobert et al. (2008) where capacitive and GPR techniques were used to evaluate the concrete cover. A number of 10 concrete slabs with dimensions of 60 × 60 × 12 cm and compressive strengths of 25 and 40 MPa were tested using a 1.5-GHz ground-coupled antenna system. The authors emphasised the importance of using the capacitive technique to provide more accurate results for the concrete cover, prior to any extensive GPR investigation. Use of a higher frequency of investigation was also suggested in order to allow for more effective measurements across the rebar offsets compatible with standard mesh grids. More recently, Zhou et al. (2018) have proven that integration of GPR with other complementary NDT methods can be a viable approach to provide more accurate information. The authors used the GPR and the EMI techniques with a maximum estimation error for the cover thickness of 6.7%. On the other hand, a difficulty in providing an effective measurement and an estimation of rebars in a densely-meshed net was identified as a limitation of the proposed approach.

4.1.5. The Assessment of Concrete Characteristics by Dielectric Properties

Several research studies are discussed in the literature in regard to the assessment of concrete characteristics by analysis of its dielectric properties. It is known that among the factors affecting the dielectric properties of a concrete material (Knoll, 1996), water is a primary and dominant parameter affecting the relative dielectric permittivity (Soutsos et al., 2001). According to Lai et al. (2009), other factors influencing the dielectric properties of concrete are: i) the EM frequency; ii) the water-to-cement ratio; iii) the porosity; iv) the ions in pore solution and v) the clay minerals with a wide range of porosity values and specific surfaces. Factors such as the cement type, the salt impregnation, the presence of pulverised fuel ash and ground granulated blast furnace slag, and the temperature during tests were reported to be of minor or negligible significance. Similarly, the effects of different types of dense aggregates on the relative dielectric permittivity were accounted to be negligible (Soutsos et al., 2001).

Louzli et al., (2002) developed a method to determine the complex dielectric permittivity of concrete mixes and to assess concrete voids. A number of five bare concrete slabs and nine slabs with a simulated delamination (simulated by placing

polystyrene plastic pieces inside the slabs) were constructed. All slabs were cast at 1.5 x 1.5 x 0.127 m and five different concrete mixes were used. Effects of delamination on the signal were analysed by way of comparison between the signals from the bare concrete slabs and the signals from the slabs with simulated delamination. In this regard, modelling the reflected signals with an average complex dielectric permittivity over the full GPR frequency range was found to provide comparable outputs in terms of synthetic and real (measured) waveforms. In addition, presence of voids located at 50 mm from the surface overlap with the surface reflection were observed to distort the shape of the reflected signal.

Several studies have investigated the EM behaviour of wet concrete. Laurens et al. (2005) analysed the effect of moisture on the radar waves propagating through concrete slabs. To this purpose, a GPR system equipped with a 1.5 GHz ground-coupled antenna was used to collect data at different degrees of saturation in homogeneous moisture distribution conditions. An investigation into the amplitudes, the velocities and the frequency spectra of the collected waveforms was developed to assess the GPR capability in estimating concrete moisture. The authors found the moisture to affect the transmitter-receiver direct wave.

GPR was also reported to characterise pore systems of air/water cured concrete through injection of continuous water over a period of 48 hours (Lai and Tsang, 2008). To this purpose, a 1 GHz radar system was used and the real part of the complex permittivity and the energy attenuation were measured. As an outcome of the investigation, it was also emphasised a good potential of GPR in identifying the progress rate of the water front in concrete walls or slabs.

Sbartai et al. (2009a) applied a combined analysis of radar technology and artificial neural networks for predicting water and chloride content of concrete. Four different concrete mixes were used to produce a number of 72 concrete slabs with dimensions of 25 × 25 × 8 cm. Moisture and chloride variations ranging from 0 to 16.5% and from 0 to 6.5 kg/m^3 were analysed, respectively. Input data to the neural networks were extracted from time domain signals of direct and back-reflected radar waves. Results highlighted the viability of using optimised statistical models to predict water and chloride content of laboratory slabs with maximum absolute errors of about 2% and 0.5 kg/m^3, respectively.

Sbartai et al. (2009b) assessed water content in concrete samples at several degrees of saturation using a frequency analysis of the direct wave signal collected from a 1.5 GHz ground-coupled antenna system. A Fast Fourier Transform algorithm was used to extract the frequency spectra of each signal and, based on the experimental results, an empirical model was proposed to relate the frequency attenuation and the concrete water content. By way of comparison between the results achieved in the time and in the frequency domains, the frequency-attenuation analysis was found to be very effective for concrete moisture assessment purposes.

Villain et al. (2010) used GPR and capacitive probes to test a number of 81 slabs made of 9 different concrete mixes. Concrete porosity ranged between 12.5 and 18% and five different water contents were reproduced. A cross-correlation model was developed and durability-related parameters such as the porosity, the water content and the chloride were

688 successfully predicted. The authors also observed that the viability of the proposed methodology is maximum if the cross-
689 correlation model is calibrated in laboratory using core samples from a real-life concrete structure.
690 Kalogeropoulos et al. (2013) proposed a multi-stage approach for the calculation of the EM parameters in concrete slabs.
691 A GPR dataset was collected using 1.2 GHz horn antennas on concrete specimens with different chloride gradients. A
692 first approach was developed to estimate the relative dielectric permittivity ε_r and the conductivity σ of the concrete.
693 Results demonstrated an accuracy of ±0.15 for ε_r and ±10mS/m for σ. A second approach, based on the use of an extended
694 full-waveform inversion forward model, enabled the creation of conductivity gradients for multi-layered media in
695 agreement with literature outcomes.
696
697 **4.2. Real-life Investigations**
698 **4.2.1.** ***Location of Reinforcing Bars***
699 Many applications of GPR exist in real-life scenarios in regard to the location of reinforcing bars and the use of GPR
700 within this specific application area was already reported by Ulriksen (1982) a few decades ago.
701 According to Hamasaki et al. (2003), the working principles of EM-based methods allow for the effective detection of a
702 wave reflected back by a reinforced bar. This is mostly due to the different dielectric properties of the two materials
703 involved. The authors argued that location, direction, and diameters of rebars can be determined based on the variations
704 of the EM field.
705 Barrile and Pucinotti (2005) used GPR to identify the position of principal and secondary (i.e. longitudinal steel bars and
706 stirrups) reinforcement bars located on the beams and columns of reinforced concrete structures. The aim of the research
707 was to assess the seismic vulnerability of a 40-year-old building. The survey was carried out using a ground-coupled
708 antenna system with a central frequency of 1.6 GHz. Longitudinal and transversal scanning were performed in order to
709 obtain a dimensional relief of the rebar position. The authors obtained detailed information on the number, position and
710 spacing of reinforcing bars. It was also possible to evaluate the thickness of the concrete covers. With a view to automation
711 and reduction of data processing times for the location of reinforcement, Shaw et al. (2005) proposed an integrated method
712 for the post-processing of GPR data using a neural network-based approach. The hyperbolic images from rebars were
713 collected using a multi-layer perceptron (MLP) network with a single hidden layer containing 8 nodes. This allowed
714 recognition of a more simplified hyperbolic shape and, hence, a lighter computational load for the algorithm. This
715 approach has proven viability in automating the identification and location of embedded steel reinforcing bars using GPR.
716 Soldovieri et al. (2006) presented an inverse scattering approach for the accurate location of rebars in reinforced concrete
717 structures. The benefit of this method is that the quality of the final output is less dependent upon the expertise of human
718 operators and, hence, less subject to interpretation errors.

719 Benedetto et al. (2012) reported the use of a multi-channel high-frequency array GPR system for the faster acquisition of
720 data in bridges. The authors provided details of rebar location using differently-polarised antennas. Stryk et al. (2013)
721 presented a comprehensive case study where positions of rebars were identified with a two-channel ground-coupled
722 antenna system with a central frequency of 1.6 GHz. Rebar positions were checked against standard requirements. More
723 recently, Seren and Saricicek (2017) carried out an on-site investigation for health monitoring purposes. The survey was
724 developed using a 2.7 GHz antenna system and migration techniques were applied to provide a correct location of the
725 reinforcing bars. Hyperbolic features were observed from 20 cm up to 1 m of depth. Stryk et al. (2017) reported a
726 comparative analysis for assessing the accuracy of GPR systems in rebar location. A number of GPR from different
727 manufacturers with antenna frequencies of 1.6 GHz were used for this purpose. The authors reported an accuracy of 10
728 mm and 5 mm in horizontal and vertical directions, respectively. It was also recommended to use a two-channel device
729 to measure the target location in two points within a single overrun and achieve additional information about the
730 orientation of rebars. Miramini et al. (2018) assessed the structural health of a 45-year-old pedestrian bridge deck after
731 the validation of the GPR technique on a strong concrete floor with known construction drawings. From the scanned
732 results, the location and orientation of the reinforcing bars were established and their diameters were estimated. The
733 signals demonstrated the absence of reinforcement corrosion or concrete damage in the form of delamination or cracking.
734

735 **4.2.2.** ***Detection of Rebar Corrosion***

736 Research in this particular application area is not as numerous for real-life scenarios as for applications carried out in a
737 laboratory environment. This is likely related to a larger difficulty encountered for the validation of research outcomes
738 by a destructive way of practice. Within this framework, focus of research was observed to be primarily directed towards
739 the development of: i) new algorithms capable to relate corrosion with specific signal features, and ii) automatic
740 algorithms for fast detection of rebar corrosion.
741 Wang et al. (2011) proposed a method for detection of rebar mat signatures in concrete bridges from GPR data using
742 partial differential equations. The aim of the research was to identify delamination within a real-life bridge deck. The
743 proposed algorithm was tested using both synthetic and real GPR images. The experimental results have proven the
744 algorithm accuracy and reliability, although weak image contrasts and low signal-to-noise ratios were found. A
745 comparison between deterioration maps for the bridge deck generated by the proposed algorithm and a traditional manual
746 method has proven the viability of the approach. The authors emphasised on the need to test the algorithm against a larger
747 GPR image dataset.
748 Martino et al. (2014) developed a method to identify thresholds relating GPR signal amplitudes and rebar corrosion. The
749 authors used GPR and the half-cell potential (HCP) method on one bridge deck removed from service, a number of 17

750 artificially-corroded slabs, and one in-service bridge deck. The HCP method was employed to measure the amount of
751 active corrosion. A significant correlation between the two NDT methods was found for each case study. Receiver
752 operating characteristic (ROC) curves were used to systematically set a threshold for the GPR and deteriorated areas of
753 the deck were identified with an accuracy of over 87% for every scenario. Abouhamad et al (2017) proposed a technique
754 based on image analysis for interpreting GPR data with the aim to create a systematic framework. Benefit of using this
755 approach was reported to overcome potential drawbacks of the numerical analysis in interpreting surface anomalies as
756 false alarms. The proposed systematic framework was supported by various GPR profiles showing several causes of
757 signal attenuation and their interpretation in regard to deterioration or rebar corrosion conditions. The approach was
758 validated on two real bridges by way of comparison between the outcomes from field visual inspections, camera images
759 and concrete core sampling. The method has proven to be accurate in identifying corrosion-related and non-corrosion-
760 related factors.
761
762 ***4.2.3. The Evaluation of the Concrete Cover***
763 The evaluation of the concrete cover has found major interest within the field for the assessment of the structural integrity
764 of civil engineering infrastructures and several case studies have been reported in the literature about the use of GPR in
765 real-life scenarios.
766 Al-Qadi and Lahouar (2005) proposed a GPR-based image-processing technique for the automatic detection of the rebar
767 parabolic signature from rigid pavements with a high-frequency ground-coupled antenna system. The authors used the
768 reflected parabolic shape to develop a theoretical reflection model with the aim of estimating the pavement dielectric
769 permittivity and the rebar depth. The algorithms were validated on GPR data collected on a known continuously
770 reinforced concrete pavement section. The technique has proven to be accurate and has showed an average error of 2.6%
771 for the estimated cover depth of rebars. Alani et al. (2013) presented an application on a road bridge with the purpose of
772 providing an accurate estimate of the concrete cover conditions. The authors observed a clear similarity between areas
773 affected by the ingress of moisture and areas with damaged concrete covers. Dinh et al. (2016) reported a substantial
774 piece of experimental research carried out on twenty-four bare concrete bridge decks using a ground-coupled 1.5-GHz
775 GPR antenna system. Identified objectives were i) to comprehend the impact of rebar depth on the GPR signal loss, ii) to
776 identify a method for providing an objective comparison of the GPR data from different bridge decks, and iii) to normalise
777 depth-amplitude effects for ensuring a more consistent assessment of bridge decks. The authors observed that mechanisms
778 governing depth-amplitude effects are mostly related to the effects of dielectric and conductive losses. However, the
779 authors concluded that specific depth-amplitude functions must be created in relation to specific overlay types in bridge
780 decks.

781

782 ***4.2.4. Structural Detailing of Anchorages and Joints in Major Structures/Infrastructures***

783 Structural detailing using GPR for assessment of the integrity of reinforced concrete structures has been reported in the
784 literature. A methodological overview on the use of GPR for surveying buildings, bridges and tunnels was given by
785 Daniels (2004). According to the author, suitability of GPR in structural inspections is mostly related to the collection of
786 reflection data from main structural boundaries. To this effect, the main boundaries to survey in a structure were identified
787 to be located at the interface between: i) a solid material and a significant void; ii) good and poor quality concrete; iii)
788 concrete and insulation materials; iv) large metal inclusions as reinforcement bars or other components; v) dry and wet
789 materials.

790 It was observed that most of the research in this specific application area was carried out over the past decade. This is
791 likely due to the fact that GPR is nowadays an established method in civil engineering and technological advances have
792 fostered its use in many challenging inspection tasks.

793 Within this framework, Hugenschmidt et al. (2010) discussed on the viability of using a high-resolution multi-sensor and
794 multi-polarised GPR system to investigate concrete retaining walls. The authors proposed two new processing methods,
795 i.e., i) a full 3D processing followed by a data fusion approach and ii) an inverse scattering followed by a data fusion
796 approach. The methods were compared with a standard processing protocol working in the two dimensions and they were
797 tested on a retaining wall in Switzerland. Results have proven the viability of the two innovative approaches. Benedetto
798 et al. (2012) used a multi-channel dual-polarised GPR system to monitor four reinforced concrete bridges. Among the
799 various findings of the research, the radar measurements provided valuable structural information on the bridge decks at
800 the joint connection between consecutive spans. Stryk et al. (2013) used a two-channel GPR system to provide accurate
801 measurements of the dowel and tie bar positions in a concrete pavement. Analyses of the GPR outputs in terms of the
802 translations of a rebar layer observed along the longitudinal axis allowed to identify an incorrect cut at the contraction
803 joints. Alani and Tosti (2018) reported a structural detailing of an "immersed tube" major tunnel type connecting a number
804 of segments at immersion joint points. Two sets of antenna systems with frequencies of 900 MHz and 2 GHz were used
805 to establish structural details of the tunnel roof at the immersion joints. The data provided ample information confirming
806 rather doubted construction design drawings/plans originally produced. The results obtained were conclusive in terms of
807 construction materials and structural design configurations (shape and dimensions) as well as the identification of rebar
808 positions at all the inspected immersion joint locations.

809

5. NEW METHODOLOGICAL AND DATA PROCESSING PROSPECTS FOR THE ASSESSMENT OF REINFORCED CONCRETE STRUCTURES USING GPR: A CASE STUDY

A higher accuracy in rebar location and an evaluation of the concrete cover can be achieved using dedicated data processing algorithms, such as migration (Chang et al. 2009), and data interpretation methods such as hyperbola fitting (Tillard and Dubois, 1995; Shihab and Al-Nuaimy, 2005). Within this framework, although a suitable level of accuracy can be reached with the available commercial software, higher precision could be required for quality control and routine inspection purposes. To speed up the data processing stage and achieve faster results, a few velocity values of propagation are usually extracted randomly from a sequence of rebar reflectors in a B-scan. This is achieved by fitting the reflections from the clearest hyperbola shapes. An average velocity is then assigned to the whole area in order to obtain a map of migrated points. In this regard, relating an average velocity value to an entire investigation area is a suitable approach for the location of rebars in relatively small reinforced concrete areas, although it might not work for large and complex environments (i.e. investigation sites with a high variation of wave propagation velocity, which is mostly unknown). The process can be improved by sampling a consistent number of targets for an estimation of velocity by the hyperbola fitting method. Accordingly, a more representative propagation velocity value can be assigned to the area for data migration purposes. In view of this, a sequence of migrated B-scans collected using a typical acquisition grid can provide high-quality C-scans and contribute to a more accurate rebar location and evaluation of the concrete cover.

Within this context, the main aim of this research is to comprehend the effect of different data sampling percentages on the estimation of a wave propagation velocity value in a reinforced-concrete-paved area with a high-dense grid mesh of rebars.

An estimation of this parameter is therefore used for data migration purposes in order to produce a viable C-scan map for a more accurate location of concrete rebars.

To achieve this aim, the following objectives are identified:

- to create a 2-D matrix of wave propagation velocity values estimated by hyperbola fitting of reflections from rebars over a whole inspected area;
- to analyse the statistical distribution of the estimated propagation velocity values and calculate the data dispersion throughout the area;
- to develop a data sampling methodology for the identification of a value of velocity of propagation representative of the entire area. This is sought by means of comparison between tomographic maps migrated at different sampling percentages (combination of longitudinal (L)/transversal (T) acquisitions and horizontal (HH)/vertical (VV) polarisations).

5.1. Methodology

A multi-stage methodology is proposed based on four main chronological steps. The data acquisition is first carried out. A second main stage is focused on the estimation of the wave propagation velocity values using the hyperbola fitting method. This allows to create a 2-D matrix of data, with dimensions of the number of rebars detected throughout the inspection area. A third stage is developed to analyse the statistical distribution of the above estimates as well as the data dispersion. Finally, a data sampling methodology is proposed to extract a representative wave propagation velocity value for data migration purposes.

5.1.1. Data Acquisition

Data were collected on a reinforced-concrete-paved area (rebar density of ~ 5 rebars/m^2) with dimensions of 1m×0.80m (Fig. 15). The IDS Aladdin GPR system equipped with a dual-polarised antenna of 2 GHz central frequency was used for testing purposes. The antenna configuration allowed to collect two different sets of data on a single scan line, as per the HH and VV polarisations. GPR signals were acquired with a horizontal resolution of 1 cm, using a time window of 32 ns and 512 samples. Longitudinal and transversal scans were performed with a scan spacing of 5 cm.

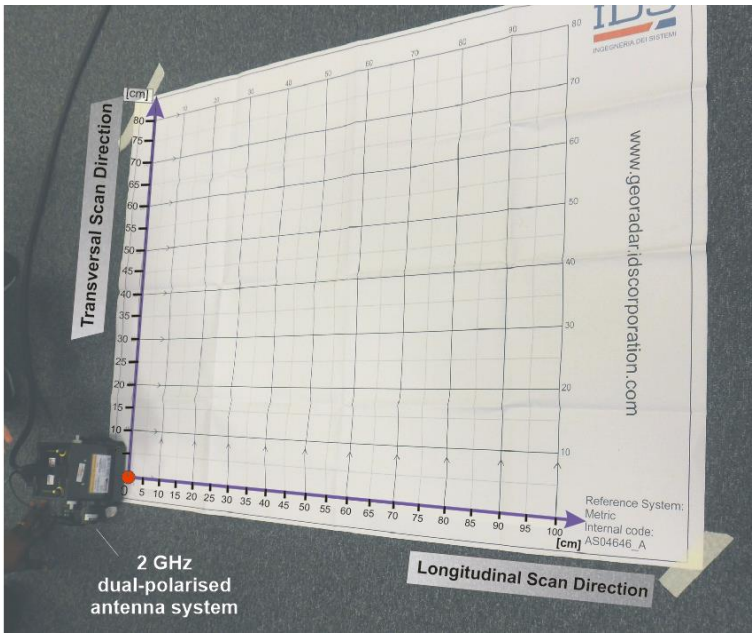

Fig. 15 Scanning grid and 2-GHz dual-polarised antenna system used for data collection purposes

5.1.2. Wave Velocity of Propagation Data Matrix by the Hyperbola Fitting Method

In view of the high-dense grid mesh of rebars and the relatively small scan spacing, the hyperbola fitting method (Shihab and Al-Nuaimy, 2005) was used to estimate the wave propagation velocity data over the whole inspected area. In this method, the wave velocity v is proportional to an angle α, formed between the hyperbola asymptotes, according to the following relationship:

$$v = 2tg\left(\frac{\alpha}{2}\right) \tag{8}$$

Several studies in the literature have proven the dependency of v on the vertex coordinates, the target radius and the time delay of the signal reflection. An example of application of the hyperbola fitting method to one of the rebars investigated in this study is reported in Fig. 16.

From the analysis of the GPR data collected on site, two main layers of rebars were observed. A number of n upper lines of rebar (being n_{max} = 5) (i.e., R1, R2, R3, R4 and R5 in Fig. 16) overlying a number of l lower lines of rebar (being l_{max} = 5) (i.e., RL1, RL2, RL3, RL4 and RL5 in Fig. 16) were collected throughout the inspection area. For the purposes of this study, only the upper rebars were taken into account. Hence, considering a scan spacing of 5 cm, m longitudinal scanning lines of 1m length (being m_{max} = 17) were collected across the 80cm-wide transversal dimension of the inspection area (Fig. 15). This turned out to provide a matrix of rebar points $\mathbf{P}_{i,j}$ sized $n \times m$ = 85 (where i stands for the "scan direction" (L, T), j stands for the "antenna orientation" (HH, VV)) and, hence, a matrix $\mathbf{V}_{i,j}$ of wave propagation velocity data with an analogous size.

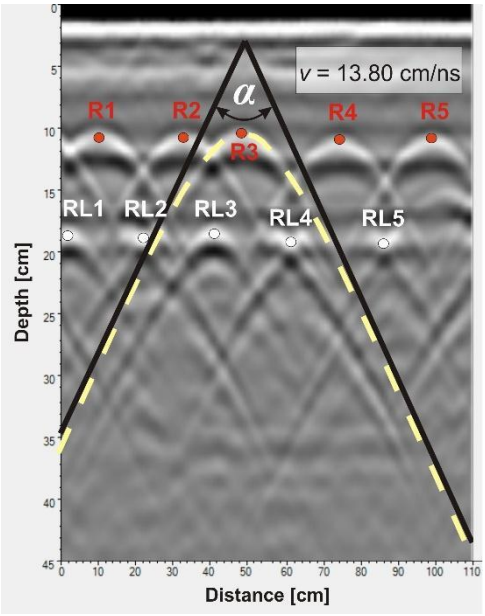

Fig. 16 Wave propagation velocity estimation on a longitudinal scan (HH polarisation). Application of the hyperbola fitting method and the B-scan layout of rebars within the inspection area (data displayed with a default v =10 cm/ns) (Tosti et al., 2018)

882

883 ***5.1.3. Statistical Distribution Analysis***

884 An analysis of the statistical distribution of the dataset of propagation velocity values $v_{i,j,k}^{[m,n]}$ (where k stands for "the
885 percentage of data collected within the inspection area") is carried out to evaluate the data dispersion within the
886 investigated area. The average value of velocity of propagation of the entire population $\overline{v_{i,j,100}}$ (value averaged over k =
887 100% of the $m \times n$ data in the propagation velocity matrix $\mathbf{V}_{i,j}$) is taken as the benchmark for every combination of the i^{th}
888 scan direction and the j^{th} antenna orientation for the calculation of the residuals. Hence, the percentage residual at a
889 random position [m, n] in the matrix $\mathbf{V}_{i,j}$ is calculated as follows:

890 $$\xi_{i,j,100}^{[m,n]} = \frac{v_{i,j,100}^{[m,n]} - \overline{v_{i,j,100}}}{\overline{v_{i,j,100}}} \times 100 \tag{9}$$

891 A matrix $\mathbf{R}_{i,j}$ of residuals $\xi_{i,j,100}^{[m,n]}$ sized $m \times n$ can be therefore computed working out the values of $v_{i,j,100}^{[m,n]}$ in Equation (8).
892 To evaluate the dispersion of propagation velocity values $v_{i,j,100}^{[m,n]}$ against the benchmark value $\overline{v_{i,j,100}}$, the m^{th} average
893 residual $\overline{\xi_{i,j,100}^{[m,n]}}$ is defined along the m = 17 scanning lines as follows:

894 $$\overline{\xi_{i,j,100}^{[m,n]}} = \sum_{n=1}^{n_{\max}} \xi_{i,j,100}^{[m,n]} \Big/ n_{\max} \qquad \forall m \in \mathbf{R}_{i,j} \tag{10}$$

895 and compared to the average residual of the entire matrix population $\overline{\xi_{i,j,100}}$ (value averaged over k = 100% of the $m \times n$
896 residuals $\xi_{i,j,100}^{[m,n]}$ in $\mathbf{R}_{i,j}$). Hence, data dispersion from this benchmark value of residuals can be interpreted as a measure of
897 non-homogeneous distribution of the propagation velocity throughout the inspection area. It is also worthy of mention
898 that this statistical analysis can be used to identify potential misalignments within a line of rebars. The frequency density
899 distributions of residuals for i) the entire matrix population $\xi_{i,j,100}^{[m\times n]}$ and ii) every n^{th} rebar $\overline{\xi_{i,j,100}^{[m,n]}}$ is also defined, being this
900 latter expressed as follows:

901 $$\overline{\xi_{i,j,100}^{[m,n]}} = \sum_{m=1}^{m_{\max}} \xi_{i,j,100}^{[m,n]} \Big/ m_{\max} \qquad \forall n \in \mathbf{R}_{i,j} \tag{11}$$

902

903 ***5.1.4. Data Sampling and Migration***

904 A number of different k^{th} percentages of $v_{i,j,k}^{[m,n]}$ values (with k = 5, 10, 15, 20, 30, 50, 50inverted) is sampled over the $n \times$
905 m data of $\mathbf{V}_{i,j}$. Sampling is developed to ensure an evenly distribution of data across the longitudinal and transversal

directions of the area (Fig. 17). The sampling configuration ranges from diagonal (i.e., smallest percentage case (Fig. 17a) to a chessboard-like arrangement at k = 50 and 50inverted (Fig. 17f-g). The optimum sampling rate of wave propagation velocity is therefore assessed by way of comparison between the migrated maps.

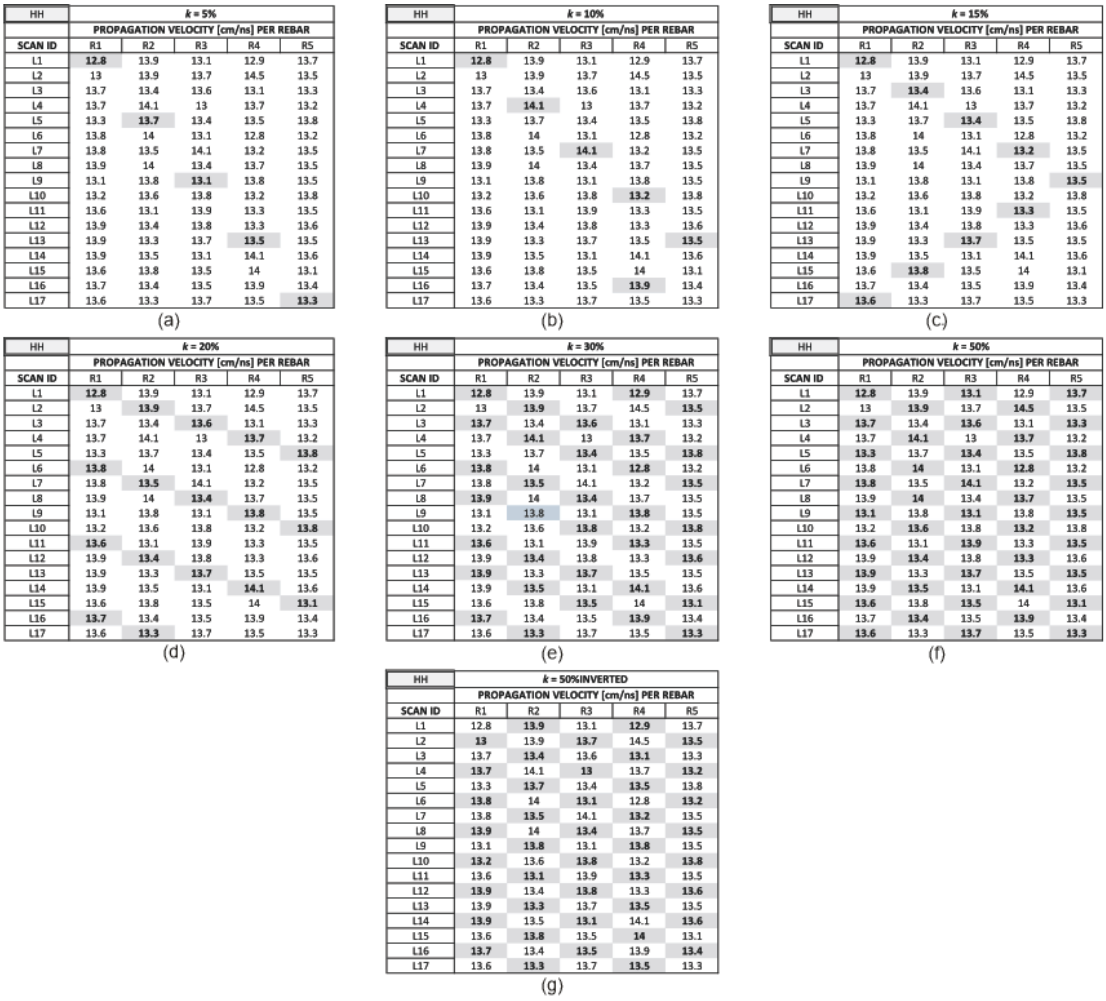

(a)

HH	k = 5%				
	PROPAGATION VELOCITY [cm/ns] PER REBAR				
SCAN ID	R1	R2	R3	R4	R5
L1	12.8	13.9	13.1	12.9	13.7
L2	13	13.9	13.7	14.5	13.5
L3	13.7	13.4	13.6	13.1	13.3
L4	13.7	14.1	13	13.7	13.2
L5	13.3	13.7	13.4	13.5	13.8
L6	13.8	14	13.1	12.8	13.2
L7	13.8	13.5	14.1	13.2	13.5
L8	13.9	14	13.4	13.7	13.5
L9	13.1	13.8	13.1	13.8	13.5
L10	13.2	13.6	13.8	13.2	13.8
L11	13.6	13.1	13.9	13.3	13.5
L12	13.9	13.4	13.8	13.3	13.6
L13	13.9	13.3	13.7	13.5	13.5
L14	13.9	13.5	13.1	14.1	13.6
L15	13.6	13.8	13.5	14	13.1
L16	13.7	13.4	13.5	13.9	13.4
L17	13.6	13.3	13.7	13.5	13.3

(b)

HH	k = 10%				
	PROPAGATION VELOCITY [cm/ns] PER REBAR				
SCAN ID	R1	R2	R3	R4	R5
L1	12.8	13.9	13.1	12.9	13.7
L2	13	13.9	13.7	14.5	13.5
L3	13.7	13.4	13.6	13.1	13.3
L4	13.7	14.1	13	13.7	13.2
L5	13.3	13.7	13.4	13.5	13.8
L6	13.8	14	13.1	12.8	13.2
L7	13.8	13.5	14.1	13.2	13.5
L8	13.9	14	13.4	13.7	13.5
L9	13.1	13.8	13.1	13.8	13.5
L10	13.2	13.6	13.8	13.2	13.8
L11	13.6	13.1	13.9	13.3	13.5
L12	13.9	13.4	13.8	13.3	13.6
L13	13.9	13.3	13.7	13.5	13.5
L14	13.9	13.5	13.1	14.1	13.6
L15	13.6	13.8	13.5	14	13.1
L16	13.7	13.4	13.5	13.9	13.4
L17	13.6	13.3	13.7	13.5	13.3

(c)

HH	k = 15%				
	PROPAGATION VELOCITY [cm/ns] PER REBAR				
SCAN ID	R1	R2	R3	R4	R5
L1	12.8	13.9	13.1	12.9	13.7
L2	13	13.9	13.7	14.5	13.5
L3	13.7	13.4	13.6	13.1	13.3
L4	13.7	14.1	13	13.7	13.2
L5	13.3	13.7	13.4	13.5	13.8
L6	13.8	14	13.1	12.8	13.2
L7	13.8	13.5	14.1	13.2	13.5
L8	13.9	14	13.4	13.7	13.5
L9	13.1	13.8	13.1	13.8	13.5
L10	13.2	13.6	13.8	13.2	13.8
L11	13.6	13.1	13.9	13.3	13.5
L12	13.9	13.4	13.8	13.3	13.6
L13	13.9	13.3	13.7	13.5	13.5
L14	13.9	13.5	13.1	14.1	13.6
L15	13.6	13.8	13.5	14	13.1
L16	13.7	13.4	13.5	13.9	13.4
L17	13.6	13.3	13.7	13.5	13.3

(d)

HH	k = 20%				
	PROPAGATION VELOCITY [cm/ns] PER REBAR				
SCAN ID	R1	R2	R3	R4	R5
L1	12.8	13.9	13.1	12.9	13.7
L2	13	13.9	13.7	14.5	13.5
L3	13.7	13.4	13.6	13.1	13.3
L4	13.7	14.1	13	13.7	13.2
L5	13.3	13.7	13.4	13.5	13.8
L6	13.8	14	13.1	12.8	13.2
L7	13.8	13.5	14.1	13.2	13.5
L8	13.9	14	13.4	13.7	13.5
L9	13.1	13.8	13.1	13.8	13.5
L10	13.2	13.6	13.8	13.2	13.8
L11	13.6	13.1	13.9	13.3	13.5
L12	13.9	13.4	13.8	13.3	13.6
L13	13.9	13.3	13.7	13.5	13.5
L14	13.9	13.5	13.1	14.1	13.6
L15	13.6	13.8	13.5	14	13.1
L16	13.7	13.4	13.5	13.9	13.4
L17	13.6	13.3	13.7	13.5	13.3

(e)

HH	k = 30%				
	PROPAGATION VELOCITY [cm/ns] PER REBAR				
SCAN ID	R1	R2	R3	R4	R5
L1	12.8	13.9	13.1	12.9	13.7
L2	13	13.9	13.7	14.5	13.5
L3	13.7	13.4	13.6	13.1	13.3
L4	13.7	14.1	13	13.7	13.2
L5	13.3	13.7	13.4	13.5	13.8
L6	13.8	14	13.1	12.8	13.2
L7	13.8	13.5	14.1	13.2	13.5
L8	13.9	14	13.4	13.7	13.5
L9	13.1	13.8	13.1	13.8	13.5
L10	13.2	13.6	13.8	13.2	13.8
L11	13.6	13.1	13.9	13.3	13.5
L12	13.9	13.4	13.8	13.3	13.6
L13	13.9	13.3	13.7	13.5	13.5
L14	13.9	13.5	13.1	14.1	13.6
L15	13.6	13.8	13.5	14	13.1
L16	13.7	13.4	13.5	13.9	13.4
L17	13.6	13.3	13.7	13.5	13.3

(f)

HH	k = 50%				
	PROPAGATION VELOCITY [cm/ns] PER REBAR				
SCAN ID	R1	R2	R3	R4	R5
L1	12.8	13.9	13.1	12.9	13.7
L2	13	13.9	13.7	14.5	13.5
L3	13.7	13.4	13.6	13.1	13.3
L4	13.7	14.1	13	13.7	13.2
L5	13.3	13.7	13.4	13.5	13.8
L6	13.8	14	13.1	12.8	13.2
L7	13.8	13.5	14.1	13.2	13.5
L8	13.9	14	13.4	13.7	13.5
L9	13.1	13.8	13.1	13.8	13.5
L10	13.2	13.6	13.8	13.2	13.8
L11	13.6	13.1	13.9	13.3	13.5
L12	13.9	13.4	13.8	13.3	13.6
L13	13.9	13.3	13.7	13.5	13.5
L14	13.9	13.5	13.1	14.1	13.6
L15	13.6	13.8	13.5	14	13.1
L16	13.7	13.4	13.5	13.9	13.4
L17	13.6	13.3	13.7	13.5	13.3

(g)

HH	k = 50%INVERTED				
	PROPAGATION VELOCITY [cm/ns] PER REBAR				
SCAN ID	R1	R2	R3	R4	R5
L1	12.8	13.9	13.1	12.9	13.7
L2	13	13.9	13.7	14.5	13.5
L3	13.7	13.4	13.6	13.1	13.3
L4	13.7	14.1	13	13.7	13.2
L5	13.3	13.7	13.4	13.5	13.8
L6	13.8	14	13.1	12.8	13.2
L7	13.8	13.5	14.1	13.2	13.5
L8	13.9	14	13.4	13.7	13.5
L9	13.1	13.8	13.1	13.8	13.5
L10	13.2	13.6	13.8	13.2	13.8
L11	13.6	13.1	13.9	13.3	13.5
L12	13.9	13.4	13.8	13.3	13.6
L13	13.9	13.3	13.7	13.5	13.5
L14	13.9	13.5	13.1	14.1	13.6
L15	13.6	13.8	13.5	14	13.1
L16	13.7	13.4	13.5	13.9	13.4
L17	13.6	13.3	13.7	13.5	13.3

Fig. 17 Data sampling (grey cells) layout of the k^{th} percentages of $v_{i,j,k}^{[n,m]}$ values in $\mathbf{V}_{i,j}$ (with i = L; j = HH; k = 5 (a), 10 (b), 15 (c), 20 (d), 30 (e), 50 (f) and 50inverted (g))

5.1.5. Results and Short Discussion

Statistical Distribution Analysis

Table 4 shows the main statistics from the wave velocity of propagation data matrices $\mathbf{V}_{i,j}$, in regard to the full set of available combinations between i (L, T) and j (HH, VV). Overall, the average value of propagation velocity $\overline{v_{i,j,100}}$ is observed to vary between 13.43 and 14.22 cm/ns across the four i^{th}, j^{th} combinations. The maximum values for the standard

deviation ($\sigma^{max}_{v_{i,j,100}}$ = 1.03 cm/ns) and the standard error ($\sigma^{max}_{\overline{v_{i,j,100}}}$ = 0.11 cm/ns) are both observed in the case of *i* = L and *j* = VV.

Table 4 Main statistics from the wave velocity of propagation data matrices $\mathbf{V}_{i,j}$

Statistic Parameter [cm/ns]	**Longitudinal Scan (*i* = L)**		**Transversal Scan (*i* = T)**	
	HH Polarisation (*j* = HH)	**VV Polarisation (*j* = VV)**	**HH Polarisation (*j* = HH)**	**VV Polarisation (*j* = VV)**
$\overline{v_{i,j,100}}$	13.54	13.58	13.43	14.22
$\sigma_{\overline{v_{i,j,100}}}$	0.04	0.11	0.10	0.06
$\sigma_{v_{i,j,100}}$	0.33	1.03	0.78	0.46
$v^{min}_{i,j,100}$	12.80	9.10	9.90	13.50
$v^{max}_{i,j,100}$	14.50	14.80	14.10	15.40

In regard to the statistics for the residual distributions, data from the longitudinal scan L / HH polarisation (*i* = L; *j* = HH) are reported in Table 5. Fig. 18 and Fig. 19 show the distribution of the average $\overline{\xi^{[m,n]}_{i,j,100}}$ and the n^{th} residual $\xi^{[m,n]}_{i,j,100}$, respectively, from the scan position *m* = 1 (0 cm on the Tscan axis) to *m* = 17 (80 cm on the Tscan axis), sorted by the n^{th} upper line of rebars.

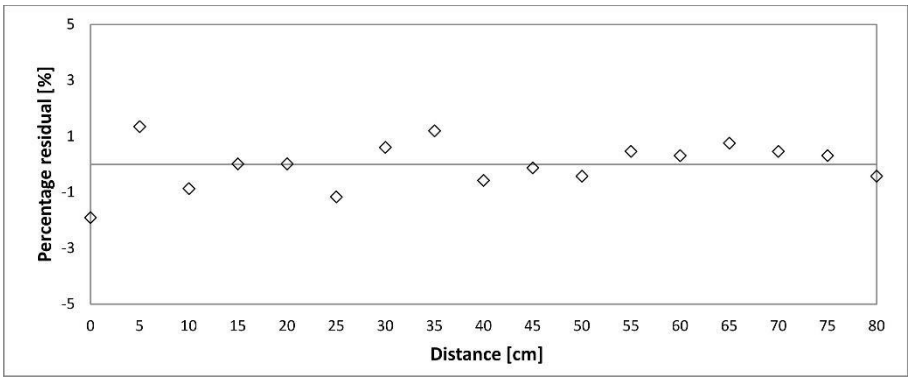

Fig. 18 Trend of the average percentage residual $\overline{\xi^{[m,n]}_{i,j,100}}$ along the *m* = 17 scan lines (Tosti et al., 2018)

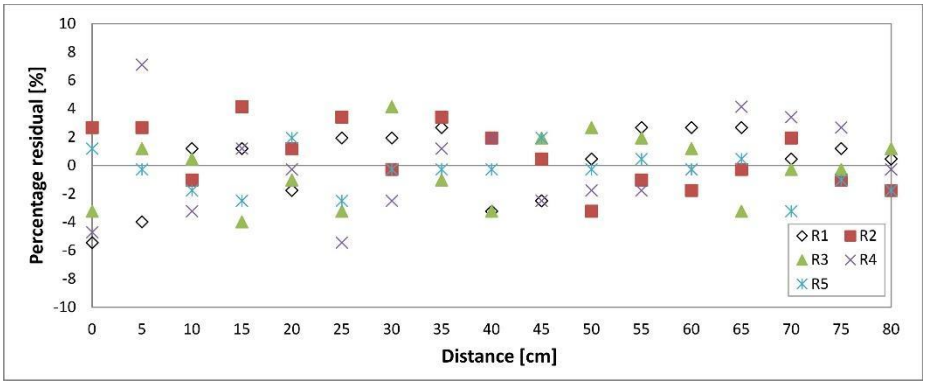

Fig. 19 Trend of the n^{th} percentage residual $\xi_{i,j,100}^{[m,n]}$ along the m = 17 scan lines (Tosti et al., 2018)

From the analysis of $\overline{\xi_{i,j,100}^{[m,n]}}$ (Fig. 18), a larger dispersion is observed from m = 1 (0 cm on the Tscan axis) to m = 7 (35 cm on the Tscan axis), as opposed to the rest of the scans. From Fig. 19, it can be noticed that the first line (n = 1; i.e., R1 in Fig. 16) and the fourth line (n = 4; i.e., R4 in Fig. 16) of rebars show the largest dispersion among the five lines investigated. On the contrary, the fifth line of rebar (n = 5; i.e., R5 in Fig. 16) has a lower variation over the benchmark $\overline{v_{i,j,100}}$, with i = L and j = HH. This evidence is confirmed by the percentage residuals $\overline{\xi_{i,j,100}^{[m,n]}}$ calculated at each n^{th} rebar in Table 5, where the rebar line R5 has the lowest statistics.

Table 5 Main statistics on the percentage residuals $\overline{\xi_{i,j,100}^{[m,n]}}$ at each rebar

Statistic Parameter [%]	**Longitudinal Scan (i = L) HH Polarisation (j = HH)**				
	R1 (n = 1)	**R2 (n = 2)**	**R3 (n = 3)**	**R4 (n = 4)**	**R5 (n = 5)**
$\overline{\xi_{i,j,100}^{[m,n]}}$	0.16	0.68	-0.28	-0.06	-0.50
$\sigma_{\overline{\xi_{i,j,100}^{[m,n]}}}$	0.62	0.53	0.59	0.80	0.36
$\sigma_{\xi_{i,j,100}^{[m,n]}}$	2.57	2.18	2.44	3.30	1.49
$\xi_{i,j,100}^{[m,n]\min}$	-5.45	-3.23	-3.97	-5.45	-3.23

$\xi_{i,j,100}^{[m,n]\max}$	2.68	4.15	4.15	7.11	1.94

Data Sampling and Migration

Data migration was applied using the average values of velocity of propagation $\overline{v_{i,j,k}^{[m\times n]}}$ at k = 5, 10, 15, 20, 30, 50 and 50inverted. To analyse the viability of the proposed sampling approach and to identify the optimal percentage of data to be used for migration purposes, the corresponding migrated C-scan tomographic maps were compared. Fig. 20 shows the C-scan tomographic maps of the inspection area obtained using data from the longitudinal scans L and the HH polarisation (i = L; j = HH). The maps are represented at a depth z = 13 cm after applying data migration at k = 10, k = 30, and k = 100.

It can be noticed that the use of a small percentage of sample data (i.e., Fig. 20a), is not sufficient to reproduce effectively the rebar configuration, as opposed to the results shown in Fig. 20c. On the other hand, the spatial sampling and the data percentage used in the case of k = 30 (i.e., Fig. 20b), indicate that a more consistent output is provided. This can turn out to provide a more accurate location of the reinforcement bars as well as a better estimation of the concrete cover in reinforced concrete structures.

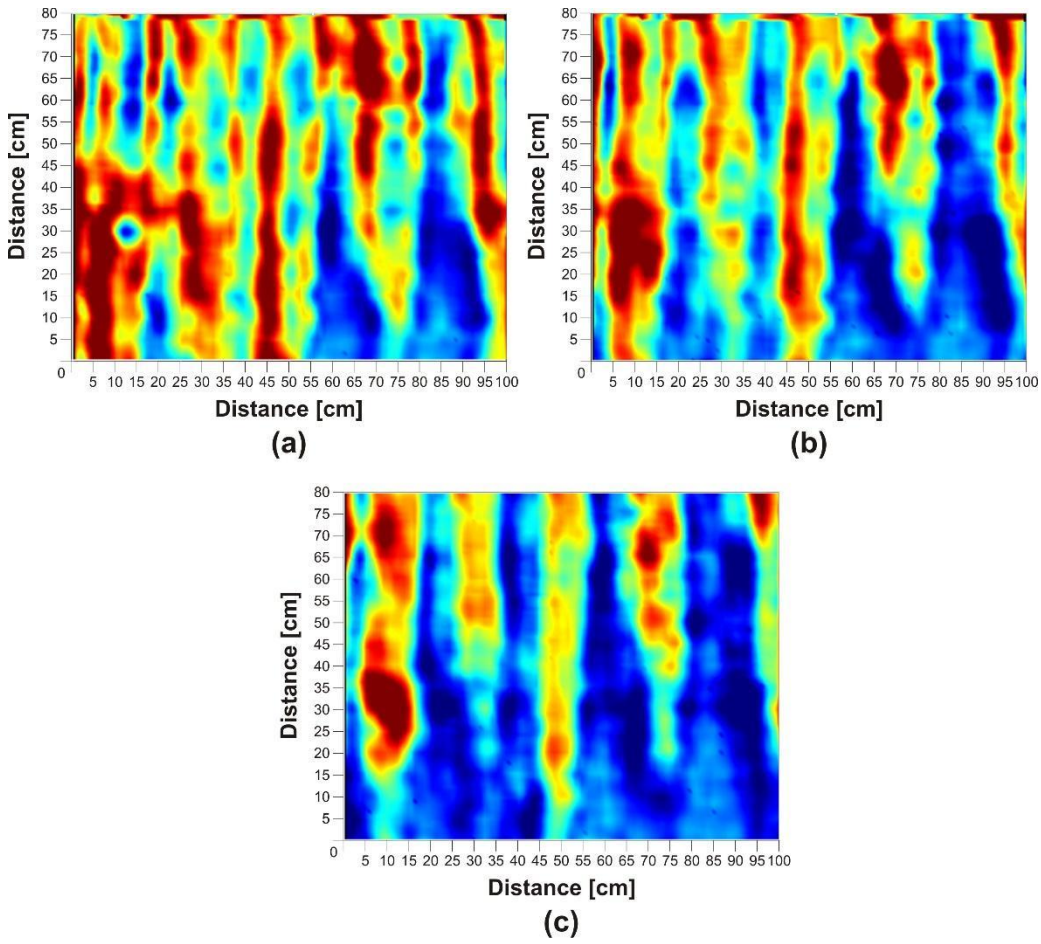

Fig. 20 C-scan maps of the area inspected (depth z = 13 cm) after the application of data migration at different k^{th} percentages of sampling. **a** k = 10, **b** k = 30, **c** k = 100 (Tosti et al., 2018)

6. CONCLUSIONS AND FUTURE PROSPECTS

In this paper, an overview of the existing literature within the subject area of Ground-Penetrating Radar (GPR) methods for the investigation of reinforced concrete structures is reported. Six major application areas have been identified where experimental, numerical and theoretical research on GPR has been developed. The review demonstrates that the applications of GPR to reinforced concrete structures are continuously growing. It was also observed that research in some application areas has been mostly or exclusively carried out at the laboratory scale and, similarly, some application areas have been investigated on real-life structures only. In terms of types of GPR systems used for purpose, existing research has been predominantly developed using pulsed-radar systems, as opposed to stepped-frequency continuous-wave (SFCW) radar systems. This was seen as being due to the higher cost of the electronics, an overall higher complexity in data processing (i.e. high computational requirements) and a lack of dedicated commercial software. Overall, ground-coupled antenna systems working in a range of nominal frequencies between 1 GHz and 2 GHz were observed to have been used across all the application areas. High-frequency GPR systems were in fact demonstrated to present a good

973 trade-off between the resolution and the depth of investigation necessary to meet the requirements of the identified
974 application areas.
975 Automation and the need for faster processing methods seem to be a major focus of the research, especially over the last
976 decade. The common high density and rather regular arrangement of rebars along with the advances achieved in
977 computational methods, have fostered the development of neural network and machine learning-based approaches. Within
978 this framework, algorithms based on full-waveform inversion models seem to be viable research avenues to pursue in the
979 near future.
980 Most common and long-standing applications have been focused on the location of rebars along with the evaluation of
981 the concrete cover, all of which were predominantly developed on real-life structures. This is due to the relatively
982 straightforward operations and data processing required to achieve the application goals. Research on the rebar corrosion
983 and on the assessment of the concrete characteristics by dielectric properties has been mostly and totally carried out in a
984 laboratory environment, respectively. This could be related to practical constraints not allowing for full control of the
985 boundary conditions, as well as to the difficulty of validating research outcomes by a destructive way of practice. On the
986 contrary, these factors are easier to control and analyse in a laboratory environment. In addition, it is worth mentioning
987 that most of the research on the dielectric properties of concrete was carried out in the 2000s for approximatively a decade.
988 The analysis of the literature review has emphasised that the estimation of the rebar size is a topical and very challenging
989 application area. Research has been performed exclusively at the laboratory scale, proving that applicability in this area
990 is at an early stage of development. A common approach is to analyse the problem using numerical modelling and validate
991 the observations with experiments carried out on samples in a laboratory environment. It was also highlighted that
992 structural detailing for the assessment of the integrity of reinforced concrete structures has gained momentum over the
993 past decade. To this effect, GPR has been demonstrated to be a viable method to achieve an early diagnosis of decay in
994 important areas, such as anchorages in building foundations and pre-stressed beams, joints in bridge decks, and tunnel
995 linings.
996 A case study on a new methodological and data processing approach for the assessment of reinforced concrete structures
997 with GPR is discussed in the final part of the paper. A data sampling investigation for the estimation of a propagation
998 velocity value representative of a reinforced-concrete-paved area with a high-density grid mesh of rebars is proposed. To
999 this purpose, a high-frequency GPR system with a 2 GHz dual-polarised antenna (HH/VV) was used and longitudinal and
1000 transversal scans were collected. A multi-stage methodology including i) data acquisition, ii) use of the hyperbola fitting
1001 method, iii) a statistical distribution analysis of the velocity values and residuals, and iv) a data sampling methodology
1002 and migration, was proposed. Results have demonstrated the advantages of using a dual-polarised GPR system in order
1003 to improve the detectability of rebars, including secondary bottom lines of reinforcement. The horizontal polarisation was

proven to be more stable compared to the vertical one. Finally, it was demonstrated that a more accurate visualisation of the rebars can be obtained using 5 cm scan spacing and information from at least 30% of the targets in a high-density grid mesh arrangement of rebars.

References

1. Abouhamad M, Dawood T, Jabri A, Alsharqawi M, Zayed T (2017) Corrosiveness mapping of bridge decks using image-based analysis of GPR data. Automation in Construction 80:104-117
2. ACI 228.2R-13 (2013) Report on Nondestructive Test Methods for Evaluation of Concrete in Structures. American Concrete Institute, Detroit
3. ACI 318 (2014) Building code requirements for reinforced concrete. American Concrete Institute, Detroit
4. Al-Qadi IL, Lahouar S (2005) Measuring rebar cover depth in rigid pavements with ground-penetrating radar. Transportation Research Record 1907:81-85
5. Alani AM, Aboutalebi M, Kilic G (2013) Applications of ground penetrating radar (GPR) in bridge deck monitoring and assessment. Journal of Applied Geophysics 97:45-54
6. Alani AM, Tosti F (2018) GPR applications in structural detailing of a major tunnel using different frequency antenna systems. Construction and Building Materials 158:1111-1122
7. Alvarez JK, Sutjipto S, Kodagoda S (2017) Validated ground penetrating radar simulation model for estimating rebar location in infrastructure monitoring. Proceedings of the 2017 12th IEEE Conference on Industrial Electronics and Applications 1460-1465
8. Annan AP (2004) Ground Penetrating Radar: Principles, Procedures & Applications. Sensors & Softwares Inc
9. ASTM C1040 / C1040M-16a (2016) Standard Test Methods for In-Place Density of Unhardened and Hardened Concrete, Including Roller Compacted Concrete, By Nuclear Methods, ASTM International, West Conshohocken, PA
10. ASTM C1150 (2002) Standard Test Method for the Break OFF Number of Concrete, Annual Book of ASTM Standards, Vol. 04.02, 640
11. ASTM C1583 / C1583M-13 (2013) Standard Test Method for Tensile Strength of Concrete Surfaces and the Bond Strength or Tensile Strength of Concrete Repair and Overlay Materials by Direct Tension (Pull-off Method), ASTM International, West Conshohocken, PA
12. ASTM C42 / C42M-18a (2018) Standard Test Method for Obtaining and Testing Drilled Cores and Sawed Beams of Concrete, ASTM International, West Conshohocken, PA

13. ASTM C597-16 (2016) Standard Test Method for Pulse Velocity Through Concrete, ASTM International, West Conshohocken, PA
14. ASTM C803 / C803M-18 (2018) Standard Test Method for Penetration Resistance of Hardened Concrete, ASTM International, West Conshohocken, PA
15. ASTM C805 / C805M-18 (2018) Standard Test Method for Rebound Number of Hardened Concrete, ASTM International, West Conshohocken, PA
16. ASTM C876 (2009) Half-cell potentials of uncoated reinforcing steel in concrete. American Society for Testing and Materials, Philadelphia
17. ASTM D4748-15 (2015) Standard Test Method for Determining the Thickness of Bound Pavement Layers Using Short-Pulse Radar, American Society for Testing and Materials
18. ASTM D4788 (2013) Detecting delaminations in bridge decks using infrared thermography, American Society for Testing and Materials
19. ASTM D6087-08e1 (2015) Evaluating Asphalt Covered Concrete Bridge Decks Using Ground Penetrating Radar, American Society for Testing and Materials
20. ASTM D6432-11 (2011) Standard Guide for Using the Surface Ground Penetrating Radar Method for Subsurface Investigation, American Society for Testing and Materials
21. ASTM D6760-16 (2016) Standard Test Method for Integrity Testing of Concrete Deep Foundations by Ultrasonic Crosshole Testing, ASTM International, West Conshohocken, PA
22. Bachiri T, Khamlichi A, Bezzazi M (2018) Detection of rebar corrosion in bridge deck by using GPR. MATEC Web of Conferences, 191:9
23. Barnes CL, Trottier JF, Forgeron D (2008) Improved concrete bridge deck evaluation using GPR by accounting for signal depth-amplitude effects. NDT & E International, 41:427-433
24. Barrile V, Pucinotti R (2005) Application of radar technology to reinforced concrete structures: a case study. NDT & E International 38:596-604
25. Beena K, Shruti S, Sandeep S, Naveen K (2017) Monitoring degradation in concrete filled steel tubular sections using guided waves. Smart Structures and Systems 19:371-382
26. Benedetto A, Manacorda G, Simi A, Tosti F (2012) Novel perspectives in bridges inspection using GPR. Nondestructive Testing and Evaluation 27:3
27. Benedetto A (2013) A three dimensional approach for tracking cracks in bridges using GPR. Journal of Applied Geophysics 97:37-44

28. Benedetto A, Tosti F, Bianchini Ciampoli L, D'Amico F (2017) An overview of ground-penetrating radar signal processing techniques for road inspection. Signal Processing
29. Billington DP (2004) Historical Perspective on Prestressed Concrete. PCI Journal 49:14-30
30. Bogas JA, Gomes MG, Gomes A (2013) Compressive strength evaluation of structural lightweight concrete by non-destructive ultrasonic pulse velocity method. Ultrasonics 53:962-972
31. Bouichou M, Marie Victoire E, Jourdan H, Thauvin B, Queguiner R, Olmi R, Riminesi C (2018) Measurement of water content and salinity index in concrete by evanescent field dielectrometry. Journal of Cultural Heritage 34:237-246
32. BS 1881-205 (1986) Testing concrete. Recommendations for radiography of concrete. British Standards Institution, London
33. BS 1881-204 (1988) Recommendations on the use of electromagnetic covermeters. British Standards Institution, London
34. BS 1881-207 (1992) Recommendations for the assessment of concrete strength by near-to-surface tests. British Standards Institution, London
35. BS 1881-208 (1996) Methods for the determination of initial surface absorption. British Standards Institution, London
36. BS 8110 (2003) Part 2 Structural use of concrete. Code of practice for special circumstances. British Standards Institution, London
37. BS EN 1542 (1999) Products and systems for the repair of concrete structures. Test methods. Measurements of bond strength by pull-off. British Standards Institution, London
38. BS EN 12504-4:2004 (2004) Testing Concrete. Determination of ultrasonic pulse velocity. British Standards Institution, London
39. BS EN 12504-1:2009 (2009) Testing concrete in structures. Cored specimens. Taking, examining and testing in compression. British Standards Institution, London
40. BS EN 12504-2 (2013). Testing concrete in structures. Non-destructive testing. Determination of rebound number. British Standards Institution, London
41. Bungey JH, Millard SG (1993) Radar Inspection of Structures. Proceedings of The Institution Of Civil Engineers. Structures And Bridges
42. Bungey JH, Millard SG, Shaw MR (1993) The influence of reinforcing steel on radar surveys of concrete structures. Construction and Building Materials
43. Bungey JH (2004) Sub-surface radar testing of concrete: a review. Construction and Building Materials 18:1-8

44. Bungey JH, Millard SG, Grantham MG (2006) Testing of concrete in structures, 4th edition, Taylor & Francis group
45. Bungey JH, Shaw MR, Millard SG, Molyneaux TCK (2003) Location of steel re-inforcement in concrete using ground penetrating radar and neural networks. Structural Faults and Repair. Engineering Technics Press London
46. Cantor TR (1984) Review of penetrating radar as applied to the non-destructive testing of concrete. American Concrete Institute 581–602
47. Carino NJ (2004) Pull-out test. Handbook on Non-destructive Testing of Concrete
48. Cassidy NJ, Eddies R, Dods S (2011) Void detection beneath reinforced concrete sections: The practical application of ground-penetrating radar and ultrasonic techniques. Journal of Applied Geophysics 74 (4):263-276
49. Chang CW, Lin CH, Lien HS (2009) Measurement radius of reinforcing steel bar in concrete using digital image GPR. Construction and Building Materials 23(2):1057-1063
50. Daniels DJ (2004) Ground-Penetrating Radar. 2nd The Institution of Electrical Engineers
51. Dérobert X, Iaquinta J, Klysz G, Balayssac JP (2008) Use of capacitive and GPR techniques for the non-destructive evaluation of cover concrete. NDT and E International 41(1):44-52
52. Dinh K, Gucunski N, Kim J, Duong TH (2016) Understanding depth-amplitude effects in assessment of GPR data from concrete bridge decks NDT and E International 83:48-58
53. Fegen I, Forde MC, Whittington HW (1979) The Detection of Voids in Concrete Piles using Sonic Methods. Colloque International sur les Méthodes de Contrôle non Destructif Grenoble
54. Fontul S, Solla M, Pajewski L (2018) Ground Penetrating Radar Investigations in the Noble Hall of São Carlos Theater in Lisbon Portugal. Surveys in Geophysics 39:1125-1147
55. Forde MC (2004) Ground penetrating radar: Introduction to Nondestructive Evaluation Technologies for Bridges. Transportation Research Board Pre-conference Workshop
56. Gagarin M, Mekemson J (2016) Step-frequency ground-penetrating-radar array calibration requirements to estimate dielectric properties of pavements. Near Surf. Geophys 14(2):105–110
57. Giannakis I, Giannopoulos A, Warren C (2019) A machine learning based fast forward solver for ground penetrating radar with application to full waveform inversion. IEEE Transactions on Geoscience and Remote Sensing. ISSN 0196-2892
58. Giannopoulos A (2005) Modelling of ground penetrating radar using GprMax. Constr Build Mater 19:755-62
59. Gizzi FT, Leucci G (2018) Global Research Patterns on Ground Penetrating Radar (GPR). Surveys in Geophysics 39(6):1039-1068

60. Grinzato E, Ludwig N, Cadelano G, Bertucci M, Gargano M, Bison P (2011) Infrared thermography for moisture detection: a laboratory study and in-situ test. Materials Evaluation 69(1)
61. Guida A, Pagliuca A, Tranquillino Minerva A (2012) A "Non-Invasive" Technique for Qualifying the Reinforced Concrete Structure. International Journal of Geophysics
62. Halabe UB, Chen HL, Bhandarkar V, Sami Z (1997) Detection of sub-surface anomalies in concrete bridge decks using ground penetrating radar. Mater J 94(5):396-408
63. Hamasaki H, Uomoto T, Ikenaga H, Kishi K, Yoshimura A (2003) Identification of reinforced in concrete by electro-magnetic methods. International Symposium Non-Destructive Testing in Civil Engineering
64. Hasan MI, Yazdani N (2014) Ground penetrating radar utilization in exploring inadequate concrete covers in a new bridge deck. Case Studies in Construction Materials 1:104-114
65. Hashemi A (2016) Microwave material characterization of alkali-silica reaction (ASR) gel in cementitious materials. Dissertation, University of Science and Technology USA
66. Hollema DA, Olson LD (2003) Crosshole Sonic Logging and Velocity Tomography Imaging of Drilled Shaft Foundations. International Symposium in Non-Destructive Testing in Civil Engineering.
67. Holt FB, Eales JW (1987) Nondestructive Evaluation of Pavements. Concrete International 9(6):41-45
68. Hubbard SS, Zhang J, Monteiro PJM, Petrson JE, Rubin Y (2003) Experimental detection of reinforcing bar corrosion using nondestructive geophysical techniques. ACI Mater 100:501-9
69. Hugenschmidt J. (2002) Concrete bridge inspection with a mobile GPR system. Construction and Building Materials 16:147–54
70. Hugenschmidt J, Loser R (2008) Detection of chlorides and moisture in concrete structures with ground penetrating radar. Mater Struct 41:785.
71. Hugenschmidt J, Kalogeropulos A, Soldovieri F, Prisco G (2010) Processing strategies for high-resolution GPR concrete inspections. NDT&E International 43:334-342
72. Kalogeropoulos A, van der Kruk J, Hugenschmidt J, Bikowski J, Brühwiler E (2013) Full-waveform GPR inversion to assess chloride gradients in concrete. NDT & E International 57:74-84
73. Kien D, Nenad G, Trung HD, Migration-based automated rebar picking for condition assessment of concrete bridge decks with ground penetrating radar. NDT & E International 98:45-54
74. Kim W, Ismail AM, Anderson NL, Atekwana EA, Buccellato A (2003) Non-destructive testing (NDT) for corrosion in bridge decks using ground penetrating radar (GPR). The 3rd International Conference on the Application of Geophysical Methodologies and NDT to Transportation Facilities and Infrastructure 8-12

75. Klysz G, Balayssa, JP, Laurens S (2004) Spectral analysis of radar surface waves for non-destructive evaluation of cover concrete. NDT E 37(3):221–227
76. Knoll MD (1996) A petrophysical basis for ground-penetrating radar and very early time electromagnetics. Dissertation, The University of British Columbia
77. Kohl C, Streicher D (2006) Results of reconstructed and fused NDT-data measured in the laboratory and on-site at bridges. Cement and Concrete Composites 28(4):402–413
78. Lachowicz J, Rucka M (2018) 3-D finite-difference time-domain modelling of ground penetrating radar for identification of rebars in complex reinforced concrete structures. Archives of Civil and Mechanical Engineering 18:1228-1240.
79. Lai WL, Tsang WF (2008) Characterization of pore systems of air/water-cured concrete using ground penetrating radar (GPR) through continuous water injection. Construction and Building Materials 22(3):250-256
80. Lai WL, Kou SC, Tsang WF, Poon CS (2009) Characterization of concrete properties from dielectric properties using ground penetrating radar. Cement and Concrete Research 39:687–695
81. Laurens S, Rhazi J, Balayssac JP, Arliguie G (2000) Assessment of corrosion in reinforced concrete by ground penetrating radar and half-cell potential tests. RILEM Workshop on Life Prediction and Aging Management of Concrete Structures
82. Laurens S, Balayssac JP, Rhazi J, Klysz G, Arliguie G (2005) Non-destructive evaluation of concrete moisture by GPR: Experimental study and direct modelling. Materials and Structures 38:827–832
83. Lee HK, Lee KM, Kim YH, Yim H, Bae DB (2004) Ultrasonic in-situ monitoring of setting process of high-performance concrete. Cement and Concrete Research 34 (4):631-640
84. Leshchinsky AM, Leshchinsky My Goncharova AS (1990) Within-test variability of some non-destructive methods for concrete strength determination. Magazine of Concrete Research 42:245–248
85. Levitt M (1969) Non-destructive testing of concrete by the initial surface absorption method. Proc Symp on NDT of Concrete and Timber 23–36
86. Loizos A, Plati C (2007) Accuracy of ground penetrating radar horn-antenna technique for sensing pavement subsurface. IEEE Sens 7(5):842–850
87. Louzli A, Al-Qadi IL, Lahouar S (2002) Ground penetrating radar signal modelling to assess concrete structures, Mater J 99(3):282-91
88. Maierhofer C, Arndt R, Röllig M, Rieck C, Walther A, Scheel H, Hillemeier B (2006) Application of impulse-thermography for non-destructive assessment of concrete structures. Cement and Concrete Composites 28(4):393-401

89. Martino N, Maser K, Birken R, Wang M (2014) Determining ground penetrating radar amplitude thresholds for the corrosion state of reinforced concrete bridge decks. Journal of Environmental and Engineering Geophysics 19(3):175-181.
90. Manning DG, Holt FB (1980) Detecting delamination in concrete bridge decks. Concrete International 2:34–41
91. McCann DM, Forde MC (2001) Review of NDT methods in the assessment of concrete and masonry structures. NDT&E International 34:71–84
92. Mechbal Z, Khamlichi A (2017) Determination of concrete rebars characteristics by enhanced post-processing of GPR scan raw data. NDT&E International 89:30–39
93. Meng D, Lin S, Azari H (2020) Nondestructive corrosion evaluation of reinforced concrete bridge decks with overlays: An experimental study. Journal of Testing and Evaluation 48:1
94. Miramini S, Sofi M, Aseem A, Baluwala A, Zhang L, Mendis P, Duffield C (2018) Health assessment of a pedestrian bridge deck using ground penetrating radar. Electronic Journal of Structural Engineering 18:30-37
95. Mishin AV (1997) Portable linear electron accelerators for electron beam curing of composites, non-destructive testing and other applications. Proceedings of the Seventh International Conference on Structural Faults & Repair 2:367–73
96. Mitchell TW (1991) Radioactive/Nuclear Methods. Handbook on Nondestructive Testing of Concrete 10:227-252
97. Moussard M, Garibaldi P, Curbach M (2017) The invention of Reinforced concrete (1848-1906) High Tech Concrete: Where Technology and Engineering Meet. Proceedings of the 2017 fib Symposium 2785-2794
98. Narayanan RM, Hudson SG, Kumke CJ (1998) Detection of rebar corrosion in bridge decks using statical variance of radar reflected pulses. Proceedings of Seventh International Conference on Ground-penetrating Radar.
99. Narayanan RM, Hudson SG, Kumke CJ, Beacham MW, Hall DD (2003) Nebraska DOR Tests GPR to Find Bridge Corrosion 73:70-73.
100. Neville AM, Brooks JJ (1987) Concrete Technology second edition.
101. Noon DA (1995) Stepped-frequency radar design and signal processing Enhances ground penetrating radar performance. Dissertation, University of Queensland St Lucia Australia.
102. Ottosen NS (1981) Nonlinear finite element analysis of pull-out test. Journal of Struct. 107:591–603
103. Patriarca C, Lambot S, Mahmoudzadeh MR, Minet J, Slob EC (2011) Reconstruction of sub-wavelength fractures and physical properties of masonry media using full-waveform inversion of proximal penetrating radar. Journal of Applied Geophysics 74:26–37
104. Plati C, Georgiou P, Loizos A (2014) Use of infrared thermography for assessing HMA paving and compaction. Transp Res Part C Emerg Technol 46:192–208

105. Popovics S, Rose JL, Popovics JS (1990) The behaviour of ultrasonic pulses in concrete. Cement and Concrete Research 20(2):259-270
106. Pucinotti R, De Lorenzo RA (2006) Nondestructive in situ testing for the seismic damageability assessment of ancient r/c structures. Book of Proceedings 3rd International Conference on NDT 189–94
107. Pucinotti R, Hinterholz L, D'Elia A, De Lorenzo RA (2007) Influence of steel reinforcement on ultrasonic pulses velocity. Book of Proceedings, 4th International Conference on NDT 189–94
108. Raju RK, Hasan MI, Yazdani N, Quantitative Relationship Involving Reinforcing Bar Corrosion and Ground-Penetrating Radar Amplitude. ACI Materials Journal 115
109. Rhim HC (2001) Condition monitoring of deteriorating concrete dams using radar. Cement and Concrete Research 31(3):363–373
110. Rhim HC, Buyukozturk O (1998) Electromagnetic properties of concrete at microwave frequency range. ACI Materials Journal 95(3):262-271
111. Rocha JHA, Santos CF, Póvoas YV (2018) Evaluation of the infrared thermography technique for capillarity moisture detection in buildings. Procedia Structural Integrity 11:107-113
112. Sbartaï ZM, Laurens S, Viriyametanont K, Balayssac JP, Arliguie G (2009) Non-destructive evaluation of concrete physical condition using radar and artificial neural networks. Construction and Building Material 23:837- 845
113. Sbartaï ZM, Laurens S, Breysse D (2009) Concrete Moisture Assessment Using Radar NDT Technique - Comparison between Time and Frequency Domain Analysis. NDTCE'09 Non-Destructive Testing in Civil Engineering Nantes
114. Sharp JH (2006) Surely we know all about cement - Don't we?. Advances in Applied Ceramics 105(4):162-174
115. Shaw MR, Molyneaux TCK, Millard SG, Taylor MJ, Bungey JH (2003) Assessing bar size of steel reinforcement in concrete using ground penetrating radar and neural networks. Insight: Non-Destructive Testing and Condition Monitoring, 45:813-816
116. Seren A, Saricicek I (2017) Investigation of concrete internal structures with GPR method. 23rd European Meeting of Environmental and Engineering Geophysics
117. Shaw MR, Millard SG, Molyneaux TCK, Taylor MJ, Bungey JH (2005) Location of steel reinforcement in concrete using ground penetrating radar and neural networks. NDT & E International 38:3
118. Shi X, Xie N, Fortune K, Gong J (2012) Durability of steel reinforced concrete in chloride environments: an overview. Construction and building materials 30:125-138
119. Shihab S, Al-Nuaimy W (2005) Radius estimation for cylindrical objects detected by ground penetrating radar. Subsurface Sensing Technologies and Applications, 6:1-16

120. Soldovieri F, Persico R, Utsi E, Utsi V (2006) The application of inverse scattering techniques with ground penetrating radar to the problem of rebar location in concrete. NDT and E International 39(7):602-607
121. Soutsos MN, Bungey JH, Millard SG, Shaw MR Patterson A (2001) Dielectric properties of concrete and their influence on radar testing. NDT&E International 34:419–425
122. Stanley CC, Balendran RV (1995) Developments in assessing the structural integrity of applied surfaces to concrete buildings and structures using infra-red thermography. Proceedings of the International Conference on Structural Faults & Repair 3:39–44
123. Stoll UW (1985) Compressive strength measurement with the Stoll tork test. Concrete International 7:42–47
124. Stryk J, Matula R, Pospisil K (2013) Possibilities of ground penetrating radar usage within acceptance tests of rigid pavements. J App Geophys 97:11-26
125. Stryk J, Matula R, Pospíšil K, Dérobert X, Simonin JM, Alani AM (2017) Comparative measurements of ground penetrating radars used for road and bridge diagnostics in the Czech Republic and France. Construction and Building Materials 154:1199-1206
126. Tillard S, Dubois JC (1995) Analysis of GPR data: wave propagation velocity determination. J Appl Geophys 33:77-91
127. Titman DJ (2001) Applications of thermography in non-destructive testing of structures. NDT & E International 34(2):149-154.
128. Tosti F, Slob E (2015) Determination, by Using GPR of the Volumetric Water Content in Structures, Substructures, Foundations and Soil, Civil Engineering Applications of Ground Penetrating Radar. Springer Transaction in Civil and Environmental Engineering
129. Tosti F, Munisami KJ, Sofroniou A, Alani AM, Benedetto F (2018) A Sampling Investigation of GPR Wave Propagation Velocity Data to Improve Migration Processing of Concrete Rebars. 41st International Conference on Telecommunications and Signal Processing (TSP)
130. Trtnik G, Kavčič F, Turk G (2009) Prediction of concrete strength using ultrasonic pulse velocity and artificial neural networks. Ultrasonics 49(1):53-60
131. Ulricksen CPF (1982) Application of impulse radar to civil engineering. Dissertation Department of Engineering Geology Lund University of Technology Sweden
132. Utsi V, Utsi E (2004) Measurement of reinforcement bar depths and diameters in concrete. Proceedings of the Tenth International Conference on Ground Penetrating Radar

133. Villain G, Dérobert X, Sbartaï ZM, Balayssac JP (2010) Evaluation of concrete water content and other durability indicators by electromagnetic measurements. Proceedings of the 13th International Conference on Ground Penetrating Radar
134. Wang ZW, Zhou M, Slabaugh GG, Zhai J, Fang T (2011) Automatic Detection of Bridge Deck Condition From Ground Penetrating Radar Images. IEEE Transactions on Automation Science and Engineering 8(3):633-640
135. Wight JK, MacGregor JG (2012) Reinforced concrete: mechanics and design. 7th Edition Pearson US
136. Wilson MA, Taylor SC, Hoff WD (1998) The initial surface absorption test (ISAT): An analytical approach. Magazine of Concrete Research 50:179-185
137. Wiwatrojanagul P, Sahamitmongkol R, Tangtermsirikul S, Khamsemanan N (2017) A new method to determine locations of rebars and estimate cover thickness of RC structures using GPR data. Construction & Building Materials 140:257-273
138. Zanzi L (2012) Modelling GPR data to understand the problems in rebar size measurements. Emerging Technologies in Non-Destructive Testing V-Proceedings of the 5th Conference on Emerging Technologies in NDT 453-457
139. Zanzi L, Arosio D (2013) Sensitivity and accuracy in rebar diameter measurements from dual-polarized GPR data. Construction and Building Materials 48:1293-1301
140. Zhou F, Chen Z, Liu H, Cui J, Spencer BF, Fang G (2018) Simultaneous estimation of rebar diameter and cover thickness by a GPR-EMI dual sensor. Sensors 6-18(9)